Eur. J. Mineral., 36, 279–300, 2024
https://doi.org/10.5194/ejm-36-279-2024

European Journal of Mineralogy
Open Access

Halogen-bearing metasomatizing melt preserved in high-pressure (HP) eclogites of Pfaffenberg, Bohemian Massif

Alessia Borghini[1,2], Silvio Ferrero[3,4], Patrick J. O'Brien[2], Bernd Wunder[5], Peter Tollan[6], Jarosław Majka[1,7], Rico Fuchs[2], and Kerstin Gresky[2]

[1]Faculty of Geology, Geophysics and Environmental Protection, AGH University of Kraków, 30-059 Kraków, Poland
[2]Institute of Geosciences, University of Potsdam, 14476 Potsdam, Germany
[3]Dipartimento di Scienze Chimiche e Geologiche, University of Cagliari, 09042 Monserrato, Italy
[4]Museum für Naturkunde (MfN), Leibniz-Institut für Evolutions- und Biodiversitätsforschung, 10115 Berlin, Germany
[5]Deutsches GeoForschungsZentrum (GFZ), 14473 Potsdam, Germany
[6]Eidgenössische Technische Hochschule, ETH, 8092 Zürich, Switzerland
[7]Department of Earth Sciences, Uppsala University, 752-36 Uppsala, Sweden

Correspondence: Alessia Borghini (borghini@agh.edu.pl)

Received: 28 June 2023 – Revised: 18 January 2024 – Accepted: 28 January 2024 – Published: 15 March 2024

Abstract. Primary granitic melt inclusions are trapped in garnets of eclogites in the garnet peridotite body of Pfaffenberg, Granulitgebirge (Bohemian Massif, Germany). These polycrystalline inclusions, based on their nature and composition, can be called nanogranitoids and contain mainly phlogopite/biotite, kumdykolite, quartz/rare cristobalite, a phase with the main Raman peak at 412 cm^{-1}, a phase with the main Raman peak at 430 cm^{-1}, osumilite and plagioclase. The melt is hydrous, peraluminous and granitic and significantly enriched in large ion lithophile elements (LILE), Th, U, Li, B and Pb. The melt major element composition resembles that of melts produced by the partial melting of metasediments, as also supported by its trace element signature characterized by elements (LILE, Pb, Li and B) typical of the continental crust. These microstructural and geochemical features suggest that the investigated melt originated in the subducted continental crust and interacted with the mantle to produce the Pfaffenberg eclogite. Moreover, in situ analyses and calculations based on partition coefficients between apatite and melt show that the melt was also enriched in Cl and F, pointing toward the presence of a brine during melting.

The melt preserved in inclusions can thus be regarded as an example of a metasomatizing agent present at depth and responsible for the interaction between the crust and the mantle. Chemical similarities between this melt and other metasomatizing melts measured in other eclogites from the Granulitgebirge and Erzgebirge, in addition to the overall similar enrichment in trace elements observed in other metasomatized mantle rocks from central Europe, suggest an extended crustal contamination of the mantle beneath the Bohemian Massif during the Variscan orogeny.

Published by Copernicus Publications on behalf of the European mineralogical societies DMG, SEM, SIMP & SFMC.

1 Introduction

Interaction between a fluid/melt phase and a rock is common during subduction and is defined as metasomatism (Harlov and Austrheim, 2013) when it causes mass transfer, i.e., gain or loss of elements in a rock, as well as mineral re-equilibration/recrystallization (see, e.g., Borghini et al., 2018, 2020). In a subduction setting, fluids and melts from the subducted crust can interact with the mantle and thus enrich it in incompatible elements and volatiles. From a geochemical standpoint, the metasomatism of the mantle wedge is a process responsible for the concentration of incompatible elements, also volatiles, in originally depleted rocks (Bebout, 2013; Klemd, 2013; Zheng and Hermann, 2014). The interaction between fluids/melts and mantle rocks can produce new phases that were not part of the original rock assemblage, such as apatite, amphibole, phlogopite and orthopyroxene (O'Reilly and Griffin, 2013). In other cases, the rock displays approximately the same mineral assemblage, but its bulk composition becomes enriched in trace elements, in particular incompatible ones (Borghini et al., 2020). In both cases, the main culprit of these changes is either a fluid or a melt. As such, the most direct way to investigate the effect of mantle metasomatism and constrain the nature of the metasomatizing agent is to study primary fluid and melt inclusions (MI), if they are present in the metasomatized rock.

Mantle metasomatism by a silicate melt with crustal origin has been investigated extensively (e.g., Zanetti et al., 1999; Malaspina et al., 2006, 2009; Vrijmoed et al., 2013; Zhao et al., 2021), but the composition of the metasomatizing agent has often been estimated indirectly, either because of the lack of inclusions or because the inclusions found in the targeted rocks do not represent the pristine agent (Malaspina et al., 2006, 2009). Many studies on metasomatizing agents were conducted in mantle xenoliths (e.g., Andersen et al., 1984; Wulff-Pedersen et al., 1996; Sajona et al., 2000; Bali et al., 2002; Matusiak-Małek et al., 2010; Puziewicz et al., 2020; Liptai et al., 2021), which however mostly record processes entirely mantle related; i.e., the metasomatizing agent is originated in the mantle without any crustal contribution. In recent years, the study of MI in metamorphic rocks originally developed in partially melted rocks (e.g., Cesare et al., 2015; Nicoli and Ferrero, 2021; Nicoli et al., 2022a) has expanded to include rocks affected by external melts, thus allowing us to describe and directly characterize the nature of metasomatizing agents, especially when the metasomatism takes place in the absence of phases which are clearly metasomatic products. Metasomatic MI were indeed recently reported and investigated in three different localities of the Bohemian Massif (Borghini et al., 2018, 2020, 2023). A crucial side product of the finding of such inclusions is the quantification of the amount of volatiles that are transferred to the mantle (Borghini et al., 2023). Carbon and H_2O are the most commonly targeted volatiles in metamorphic MI studies due to their crucial influence on metamorphic processes (Bartoli et al., 2014; Carvalho et al., 2020) as well as planetary-scale volatile cycles (Nicoli et al., 2022b). However, halogens such as Cl and F play an equally important role in deep geological processes, as they enhance the capability of deep melts and fluids to transport both metals (Lamadrid and Steele-MacInnis, 2021) and other trace elements (Harlov and Aranovich, 2018), besides extending the stability fields of some hydrous mineral phases (e.g., biotite) towards higher temperatures (e.g., Antignano and Manning, 2008; Aranovich et al., 2013; Harlov and Aranovich, 2018; Ferrero et al., 2021a).

In this contribution we provide new petrological and geochemical data on a metasomatizing agent trapped as primary MI in garnets from two different eclogite lenses enclosed in the garnet peridotite body of Pfaffenberg, Waldheim (Germany). We performed a MI study using multiple techniques – optical microscopy, micro-Raman spectroscopy, electron microprobe (EMP) and laser ablation inductively coupled plasma mass spectrometry (LA-ICP-MS) – which allowed us to retrieve the composition of the melt and its volatile content and to gain insights into the nature of the source rock. Through this study we provide important novel data on the storage of volatiles, halogens in particular, in the mantle beneath the Bohemian Massif during the subduction of the Variscan continental crust.

2 Geological setting

The collision of Laurasia and Gondwana produced the Variscan orogenic belt, a mountain range of 8000 km extending across Europe (e.g., O'Brien and Carswell, 1993; O'Brien, 2000). The high-grade crystalline core of this orogen is exposed in the Bohemian Massif (O'Brien and Carswell, 1993). The evolution of this massif can be divided into two subduction stages – first involving oceanic crust ($\sim$ 380 Ma) and then continental crust ($\sim$ 340 Ma) – followed by continent–continent collision and late granitoid intrusions ($\sim$ 310; e.g., Franke, 2000; O'Brien, 2000; Scott et al., 2013; Schulmann et al., 2014). The two main tectonic units containing the high-grade crystalline core of the Bohemian Massif are the Moldanubian and the Saxothuringian zones. Both units contain high-grade eclogites, granulites and garnet peridotites (O'Brien, 2000, 2006), and both show ultrahigh-pressure (UHP) metamorphism, i.e., in coesite and diamond stability fields (Moldanubian Zone: Naemura et al., 2011; Perraki and Faryad, 2014; Saxothuringian Zone: Nasdala and Massonne, 2000; Massonne, 2001; Kotková et al., 2011; Schönig et al., 2021).

The samples investigated here come from the Saxothuringian Zone, more specifically from the Saxonian Granulitic Complex or Granulitgebirge (Fig. 1a). The Granulitgebirge represents a slice of continental crust subducted to mantle depth and then rapidly exhumed and cooled at mid-crustal levels (O'Brien and Rötzler, 2003; Rötzler et al., 2008). This complex is a NE–SW elongated dome

20 km wide and 50 km long located in the northwestern part of the Saxothuringian Zone. It is dominated by HP quartzo-feldspathic granulites and minor layers of intermediate to basic pyroxene-bearing granulites (e.g., O'Brien and Carswell, 1993; O'Brien, 2000, 2006, 2008; O'Brien and Rötzler, 2003; Rötzler et al., 2008; Schmädicke et al., 2010). The granulites host bodies of garnet- and spinel-bearing peridotites, now almost completely serpentinized, deformed and oriented parallel to the main foliation in the granulites. In turn, these bodies contain layers and lenses of pyroxenites and eclogites (e.g., O'Brien and Carswell, 1993; Massonne and Bautsch, 2002; O'Brien, 2008; Rötzler et al., 2008; Schmädicke et al., 2010; Borghini et al., 2018, 2020). All these lithologies represent the deepest structural units in the area, and they are separated from the shallowest structural unit, the Schist Cover, by a detachment fault. The Schist Cover was metamorphosed during the emplacement of the granulites, and it is characterized by low-pressure–high-temperature (LP–HT) assemblages (O'Brien and Carswell, 1993; Reinhardt and Kleemann, 1994). Cordierite- and garnet-rich paragneisses, metamorphosed ophiolitic lithologies, and orthogneisses can locally occur between the granulites and the Schist Cover. Late monzogranite intrusions crosscut all the above lithologies (O'Brien, 2000; Rötzler et al., 2008; Schmädicke et al., 2010).

The conditions of peak metamorphism estimated for the granulites and garnet clinopyroxenites, in general, are 1000–1015 °C and 2.0–2.2 GPa (Rötzler et al., 2008; Hagen et al., 2008), and the granulite peak stage was dated to ca. 340 Ma (Rötzler and Romer, 2001). However, in the locality of Waldheim, some keliphitic spinel peridotites – a strongly retrogressed version of the garnet peridotites – show peak metamorphic conditions of ∼ 990–1000 °C and 2.6 GPa (Schmädicke et al., 2010), thus supporting the possibility that these rocks indeed experienced re-equilibration at a depth higher than what was recorded by the surrounding granulites.

3 Methods

Rock samples were collected from two different eclogite lenses. They were then investigated in detail in three thin sections and two double-polished thick sections (∼ 150 µm) with a polarized light optical microscope at the University of Potsdam to determine the mineral assemblage and select inclusion-bearing garnets. Sample preparation, microstructural observation, micro-Raman spectroscopy and chemical analyses on mineral phases, and re-homogenized inclusion analyses were performed at the University of Potsdam.

The whole rock was analyzed in an external facility, the Bureau Veritas Mineral Laboratories in Vancouver. The sample was crushed and analyzed with X-ray diffraction (XRD) for major elements and with an inductively coupled plasma mass spectrometer (ICP-MS) for trace elements (TEs).

A total of 80 inclusions hosted in six garnets from two thin sections were investigated via micro-Raman spectroscopy, backscattered electron (BSE) imaging, energy dispersive X-ray (EDS) elemental mapping and electron microprobe analyses (EMPA). The main mineral assemblage in the MI was determined via micro-Raman spectroscopy using a Horiba Jobin-Yvon LabRAM HR 800 furnished with a Peltier-cooled multichannel CCD detector and an Olympus BX41 confocal optical microscope. The air-cooled Nd:YAG laser was used for the excitation ($\lambda = 523$ nm with laser power of 2–3 mW). The spectra were acquired with the 100× objective; the grating of 300 lines mm^{-1}; the multiwindow option in the 100–4000 cm^{-1} range; and integrating three repetitions of 10 s, yielding a measurement time of 3 min per spectrum with a spectral resolution of ∼ 10 cm^{-1} (for details see Ferrero et al., 2015). The laser power on the sample was reduced by a neutral glass filter to 25 %, the slit width was set to 100 µm and the confocal hole was set to 200 µm. An electron microprobe, JEOL JXA-8200, was used for the determination of the chemical composition of the mineral phases and the melt in the inclusions. The measurements of the mineral phases were performed with an acceleration voltage of 15 kV, a current of 15 nA and a beam diameter of 2 µm. Apatite was analyzed with the same setup described above, but the beam diameter was increased to 5 µm, F and Cl were analyzed in the first run, and the acquisition time for these two elements was reduced with respect to the others. Moreover, the analyses were alternated with measurements of two different standard apatites: the USNM 104021 Durango was used for Cl and Astimex MINM25–35 was used for F. The analyses on the phases in the MI were performed with a diameter of 1 µm to avoid contamination from the surrounding phases or the host. The glassy re-homogenized inclusions were analyzed with the same diameter but with a current of 3.5 nA (with a detection limit for Cl of ∼ 100–80 ppm). For these analyses, the microprobe was calibrated with hydrous leucogranitic standards with H_2O content similar to the glassy inclusions. The standard glass was also used as a reference for the correction of Na, K, Al and Si because of the common loss of alkalis in granitic melts during analysis (Morgan and London, 2005). The elemental maps of the inclusions and the BSE images were carried out using a field emission gun electron microprobe (FEG-EMP) and a JEOL JXA-8500F hyperprobe, at the Deutsches GeoForschungsZentrum (GFZ) in Potsdam. The instrument was set with an acceleration voltage of 15 kV and a current of 5 nA.

In order to determine the composition of the melt, nanogranitoids were re-homogenized to glass with a piston cylinder apparatus (type: Boyle and England) at the GFZ, Potsdam. Different P–T conditions were used in order to find those close to entrapment, thus aiming to obtain a complete homogenization to glass with no host–inclusion interaction and formation of new phases or shrinkage bubbles within the inclusions (see Sect. 4.4 for details and Table S1 in the Supplement). Selected melt-inclusion-bearing garnet

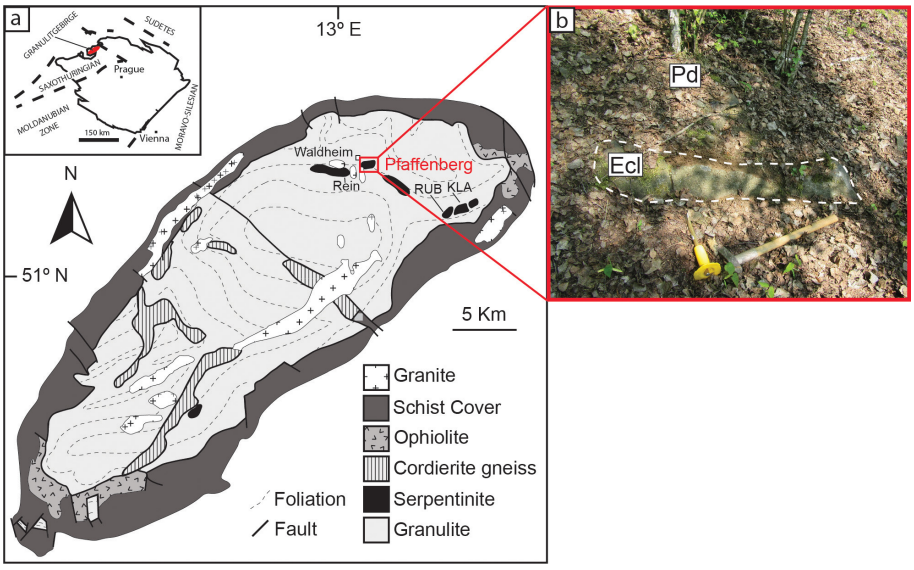

Figure 1. Schematic geological map of the Granulitgebirge (modified after Rötzler et al., 2008; Borghini et al., 2020). The study area is reported in red along with the other localities with similar eclogites, Rubinberg (RUB) and Klatschmühle (KLA) previously investigated by Borghini et al. (2018, 2020). **(a)** Inset with the location of the Granulitgebirge in the Bohemian Massif. **(b)** Field picture of the outcrop in Pfaffenberg where a lens of eclogite (Ecl) is enclosed in serpentinized garnet peridotites (Pd).

chips were mechanically removed from two double-polished thick sections and inserted in a platinum capsule (4 mm long and with a diameter of 3 mm) together with quartz powder – in order to separate the garnet chips from each other and from the capsule walls. The latter was then cold sealed and embedded in crushable alumina (Al_2O_3) and then in a talc–pyrex–graphite assemblage. The experiments were performed in two steps: first compression and then heating under dry conditions for 24 h. Pressure calibration was made using the quartz–coesite transition with an accuracy of $\pm$ 0.05 GPa, whereas the temperature was controlled with a K-type thermocouple (Ni/CrNi) with an accuracy of $\pm$ 10 °C. Each experiment was quenched, and the Pt capsule was mounted in epoxy and polished to expose the re-homogenized inclusions within the garnet chips.

Trace element (TE) contents were measured on nanogranitoids located below the sample surface and not re-homogenized. TEs were determined with LA-ICP-MS at the Department of Earth Science, ETH Zürich. We used the COMPexPro 102 excimer laser (193 nm) with a repetition rate of 10 Hz, fluency on the sample of 8 J cm^{-2} and a small volume cell for fast washout. A total of 60 inclusions belonging to five garnet chips were analyzed with variable spot sizes (20–60 µm) depending on the size of the inclusions and always using a slightly bigger diameter to successfully ablate the entire volume of the inclusion. Helium with a flow rate of 1.0 L min^{-1} transported the ablated material, and it was mixed with argon before entering the ICP-MS. The latter is a Thermo Scientific Element XR, operating in low-mass-resolution mode with counting times for most elements between 11 and 20 ms. The following isotopes have been recorded: ^{7}Li, ^{11}B, ^{23}Na, ^{24}Mg, ^{27}Al, ^{29}Si, ^{31}P, ^{39}K, ^{43}Ca, ^{45}Sc, ^{49}Ti, ^{51}V, ^{53}Cr, ^{55}Mn, ^{57}Fe, ^{59}Co, ^{62}Ni, ^{65}Cu, ^{66}Zn, ^{85}Rb, ^{88}Sr, ^{89}Y, ^{90}Zr, ^{93}Nb, ^{95}Mo, ^{118}Sn, ^{133}Cs, ^{137}Ba, ^{139}La, ^{140}Ce, ^{141}Pr, ^{146}Nd, ^{147}Sm, ^{151}Eu, ^{157}Gd, ^{159}Tb, ^{163}Dy, ^{165}Ho, ^{166}Er, ^{169}Tm, ^{173}Yb, ^{175}Lu, ^{178}Hf, ^{181}Ta, ^{182}W, ^{208}Pb, ^{232}Th and ^{238}U. In order to calculate for drift correction and quantify the analyses, we used NIST SRM 610 as glass reference standard material (Jochum et al., 2011), whereas we additionally used USGS glasses (GSD-1G and GSE-1G) to verify analytical accuracy. The reference materials were ablated with the same conditions used for the inclusions, and the software SILLS was used to process the acquired time-integrated signals (Guillong et al., 2008). With this method, both the inclusion and the host contribute to the signal, and thus a deconvolution is applied (Halter et al., 2002). The average Na_2O content measured in the melt via EMPA (Table 4) was used as an internal standard (inclusion-dominated tracer), whereas MgO was used as a matrix-only tracer. Moreover, due to the methods used, the number of elements highly enriched in the host, such as heavy rare earth elements (HREE) and Y, cannot be quantified for the investigated melt.

The F concentration in the melt was not quantified via EMPA because it was expected to be close to or below the detection limit of the instrument. It was thus calculated using the F partitioning coefficient between apatite and melt after measuring the F content in the apatite coexistent with the melt. This partitioning is non-Nernstian, i.e., non-linear, and requires a thermodynamic model to be determined (Li

and Hermann, 2017).

$$K_{\mathrm{dF\text{-}OH}}^{\mathrm{Ap\text{-}melt}} = \exp\left\{\left[-\Delta_r G^0_{\mathrm{F\text{-}OH}}(P,T) + \left(X_{\mathrm{F}}^{\mathrm{Ap}} - X_{\mathrm{OH}}^{\mathrm{Ap}}\right) W_{\mathrm{F\text{-}OH}}^{\mathrm{Ap}} + X_{\mathrm{Cl}}^{\mathrm{Ap}}\left(W_{\mathrm{Cl\text{-}OH}}^{\mathrm{Ap}} - W_{\mathrm{F\text{-}Cl}}^{\mathrm{Ap}}\right)\right] \times \frac{\frac{10^3}{8.314}}{T}\right\} \quad (1)$$

The values for $-\Delta_r G^0_{\mathrm{F\text{-}OH}}(P,T)$, $W_{\mathrm{F\text{-}OH}}^{\mathrm{Ap}}$, $W_{\mathrm{Cl\text{-}OH}}^{\mathrm{Ap}}$ and $W_{\mathrm{F\text{-}Cl}}^{\mathrm{Ap}}$ were taken from Li and Hermann (2017). The equation was calibrated for 800 °C and 2.5 GPa, and the P–T conditions for MI entrapment were based on our piston cylinder experiments (see below).

4 Results

4.1 Petrography

The eclogites investigated in the present work crop out on the side of a railway track near the Museumsgaststätte Pfaffenberg in Waldheim (GPS coordinates: 51.068586, 13.015201). In the field we identified three discontinuous lenses of eclogites (∼ 1 m long and 20 cm thick) hosted in a garnet peridotite body (Fig. 1b). The rock is granoblastic and dominated by garnet and clinopyroxene, with a minor amount of plagioclase, brown amphibole and biotite and, as accessories, apatite, rutile and ilmenite (Fig. 2a–b). Amphibole, biotite and plagioclase have been interpreted as post-peak, retrograde phases. Garnet is a few millimeters in diameter and includes mainly clinopyroxene, rutile, ilmenite, plagioclase, apatite and primary MI. Clinopyroxene is present both in the matrix and as inclusion in garnet, and in most cases, it has cloudy cores with albite exsolution and clear rims. Clinopyroxene is often surrounded by symplectites of plagioclase + orthopyroxene ± ilmenite. Apatite has cloudy cores due to the presence of nanometric CO_2 inclusions (verified via micro-Raman spectroscopy), and it occurs either as inclusions in garnet or in the matrix, often associated with brown amphibole, ilmenite and locally also biotite (Fig. 2c). In general, the eclogites targeted for investigation in this contribution are very similar to the eclogites of Rubinberg (RUB) and Klatschmühle (KLA), located approximately 10 km E-SE with respect to Waldheim and investigated in detail by Borghini et al. (2018, 2020). The latter two case studies are used throughout this work as the main term of comparison for the present case study.

4.2 Whole-rock and mineral chemistry

Pfaffenberg (PF) samples are similar to RUB and KLA eclogites in terms of bulk chemical composition in both major and trace elements (Fig. 3 and Table S2 in the Supplement; Borghini et al., 2020). The only striking difference is related to the P_2O_5 content, 1.25 wt % versus 0.12 wt % and 0.16 wt % for RUB and KLA respectively. In terms of TEs, Pfaffenberg bulk is enriched in large ion lithophile elements (LILE; Cs in particular), Th, U, Zr, Hf and Ti with negative Sr, Nb, Pb and Ta anomalies (Fig. 3b), similarly to what is observed for RUB and KLA. At Pfaffenberg the bulk rock is more enriched in light rare earth elements (LREE) and P than the aforementioned eclogites, and it shows a negative anomaly of Pb, as is also visible for the Klatschmühle samples (Fig. 3b).

Similarly to what has been observed for the whole rock, the mineral phases are also very much like those in the RUB and KLA eclogites (Fig. 3a). Garnet generally is homogeneous and contains similar amounts of MgO and FeO and slightly less CaO, with an average pyrope (Prp) of 37 mol %, almandine (Alm) 37 mol %, grossular (Grs) 25 mol % and spessartine (Sps) 1 mol % and a Mg# of 50 (Table 1). Clinopyroxene displays a variable content of Na_2O, and its jadeite (Jd) content ranges from 20 mol % on average for the clinopyroxene included in garnet (Mg# = 73) to ∼ 13 mol % in the matrix of the less altered samples (Table 1) to 7 mol %–3 mol % for the clinopyroxene surrounded by more pervasive symplectites. The composition of the clinopyroxene included in garnet is similar to that in the Klatschmühle samples. In the Bohemian Massif, rocks very similar to those investigated here were generally reported as garnet clinopyroxenites in older literature (Schmädicke et al., 2010, and references therein). We defined them as eclogites due to the fact that they display higher Na_2O and TiO_2 and lower Cr, Ni and Mg# than garnet clinopyroxenites, once again similarly to the RUB and KLA eclogites; the reader is also referred to Borghini et al. (2020) for a detailed discussion on the criteria used to differentiate eclogites and garnet clinopyroxenites. Apatites are H_2O-rich with an average H_2O content of ∼ 2.0 wt % and poorer in both F and Cl, with F of ∼ 1.0 wt % and Cl slightly variable with 0.79 wt % for apatite in garnet and 0.70 wt % for the ones in the matrix.

4.3 Melt inclusions

Garnet contains, in its inner part, MI randomly distributed in wide clusters (Fig. 2d). The inclusions are up to 30 µm in diameter; they display a well-developed negative crystal shape; and they consist of a cryptocrystalline assemblage dominated by quartz/cristobalite, two feldspars and phyllosilicates typical of nanogranitoids (Cesare et al., 2015). The investigation with micro-Raman spectroscopy, EDS mapping and EMP revealed the presence of phlogopite/biotite, kumdykolite (orthorhombic polymorph of $NaAlSi_3O_8$; Ferrero et al., 2016), quartz/rare cristobalite, a phase with the main Raman peak at 412 cm^{-1}, a phase with the main Raman peak at 430 cm^{-1}, chlorite, osumilite and plagioclase (Fig. 4; Table 2). White mica, K-feldspar, amphibole and kokchetavite (hexagonal polymorph of $KAlSi_3O_8$; Ferrero et al., 2016) are also present in minor amounts. Clinopyroxene occurs in inclusions as a trapped phase, and chlorite is abundant in de-

Table 1. Averages of garnet, clinopyroxene and apatite electron microprobe analyses of three thin sections of Pfaffenberg eclogites (garnet: almandine – Alm, pyrope – Prp, spessartine – Sps, grossular – Grs; clinopyroxene: jadeite – Jd, quadrilateral – Quad (Ca–Mg–Fe^{2+} pyroxenes), aegirine – Ae). Clinopyroxene and apatite were analyzed in the matrix and included in the garnet.

Locality	Pfaffenberg											
Phase	Garnet			Clinopyroxene			Apatite					
Sample name	PF 4.1	PF 5.1	PF 5.2	PF 5.1	PF 5.1	PF	PF 5.1	PF 5.2	PF 4.1	PF 5.1	PF 5.2	PF 4.1
Mineral	Grt	Grt	Grt	Cpx1	Cpx2	Cpx in Grt	Ap in Grt	Ap in Grt	Ap in Grt	Ap in matrix	Ap in matrix	Ap in matrix
No. of analyses	16	13	12	11	3	15	59	30	24	63	66	70
wt %												
SiO_2	39.39	38.7	39.42	47.32	48.69	49.47	0.26	0.14	0.32	0.2	0.19	0.33
TiO_2	0.17	0.21	0.20	0.90	0.88	0.79	–	–	–	–	–	–
Al_2O_3	22.76	22.82	22.59	11.46	11.65	12.30	0.07	0.01	0.10	0.04	0.03	0.08
Cr_2O_3	0.02	0.05	0.05	0.02	0.03	0.03	–	–	–	–	–	–
Fe_2O_3	–	–	–	–	–	–	–	–	–	–	–	–
FeO	18.52	17.53	17.43	7.99	7.70	6.59	0.54	0.51	0.53	0.24	0.21	0.3
MnO	0.41	0.36	0.36	0.08	0.09	0.06	0.02	0.02	0.03	0.03	0.02	0.04
MgO	10.76	9.81	9.79	10.74	10.50	9.96	0.20	0.16	0.26	0.08	0.08	0.11
CaO	8.20	10.41	10.32	18.84	19.22	17.87	53.86	54.2	53.75	54.26	54.32	54.09
Na_2O	0.03	0.03	0.05	2.32	2.35	3.52	0.22	0.23	0.24	0.16	0.2	0.23
P_2O_5	0.09	0.07	0.07	0.02	0.03	0.02	40.87	40.91	40.84	41.2	41.09	40.99
F	–	–	–	–	–	–	1.11	1.18	1.16	0.98	1.11	1.22
Cl	–	–	–	–	–	–	0.86	0.83	0.55	0.79	0.77	0.57
Total	100.35	99.99	100.28	99.69	101.14	100.61	98.01	98.19	97.78	97.98	98.02	97.96
Mg#	51	50	50	71	71	73	–	–	–	–	–	–
Si	2.95	2.92	2.96	1.74	1.76	1.78	0.04	0.02	0.05	0.03	0.03	0.06
Ti	0.01	0.01	0.01	0.02	0.02	0.02	–	–	–	–	–	–
Al	2.01	2.03	2.00	0.49	0.50	0.53	0.01	0.00	0.02	0.01	0.01	0.02
Cr	–	–	–	0.00	0.00	0.00	–	–	–	–	–	–
Fe^{2+}	1.16	1.11	1.10	0.10	0.14	0.09	0.08	0.07	0.08	0.03	0.03	0.04
Fe^{3+}	–	–	–	0.14	0.09	0.11	–	–	–	–	–	–
Mn	0.03	0.02	0.02	0.00	0.00	0.00	0.00	0.00	0.00	0.00	0.00	0.01
Mg	1.20	1.11	1.10	0.59	0.57	0.54	0.05	0.04	0.07	0.02	0.02	0.03
Ca	0.66	0.84	0.83	0.74	0.75	0.69	9.94	10.00	9.92	10.01	10.02	9.98
Na	–	–	–	0.16	0.16	0.25	0.07	0.08	0.08	0.05	0.07	0.08
P	–	–	–	–	–	–	5.96	5.96	5.95	6.01	5.99	5.98
F	–	–	–	–	–	–	0.6	0.64	0.63	0.54	0.60	0.67
Cl	–	–	–	–	–	–	0.25	0.24	0.16	0.23	0.22	0.17
OH	–	–	–	–	–	–	1.14	1.11	1.21	1.24	1.17	1.17
mol %												
Alm	38	36	36									
Prp/Jd	39	36	36	12	14	20						
Sps/Quad	1	1	1	81	81	73						
Grs/Ae	22	27	27	7	5	7						

crepitated inclusions, i.e., inclusions surrounded by cracks. Nanogranitoids also locally contain graphite, calcite, apatite, rutile and a fluid phase rich in CO_2, CH_4 and locally N_2 (Fig. 4e), when measured under the surface of the sample.

Kumdykolite was analyzed in six inclusions, and its composition is on average $Ab_{77}An_{22}Or_1$, varying from $Ab_{87}An_{12}Or_2$ to $Ab_{67}An_{29}Or_3$ (Table 2). Three analyses acquired of osumilite show high amounts of SiO_2, Al_2O_3 and MgO and additionally minor contents of FeO and K_2O. Biotite is mostly present as phlogopite and is thus Mg-rich, but locally Fe-rich biotite was also identified (Table 2). Chlorite is instead present only as Mg-rich clinochlore. Representative Raman spectra of the phases in nanogranitoids are available in the Supplement (Fig. S1).

The two phases characterized by main peaks at 412 and 430 cm^{-1} are almost ubiquitous in PF nanogranitoids (Fig. 5). Micro-Raman spectroscopy shows that phase 412 has a simple spectrum with two secondary peaks at 105 and 831 cm^{-1} and a weaker peak at 470 cm^{-1} (Fig. 5c). The Raman spectrum of phase 430 is instead more complex and displays, besides the main peak at 430 cm^{-1}, a strong peak at 292 cm^{-1}; secondary peaks at 128 and 182 cm^{-1}; and weaker peaks at 240, 480, and 820 cm^{-1} (Fig. 5d). Both spectra do not correspond to available published data on phases commonly found in melt and fluid inclusions (Frezzotti et al., 2012) or to data from online databases of Raman spectra (e.g., RRuff). They are thus likely to represent new phases, and for this reason they are presently under further investigation (Ferrero et al., 2023). Interestingly, the

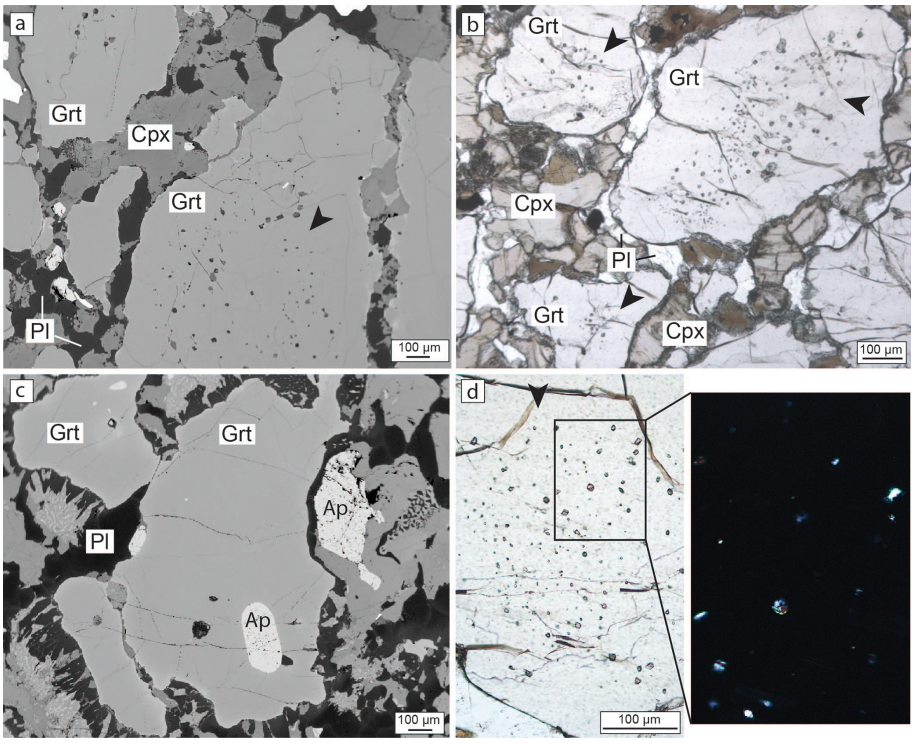

Figure 2. Backscattered electron (BSE) images **(a, c)** and parallel **(b, d)** and crossed-polars **(d)** photomicrographs of Pfaffenberg eclogites displaying the distribution of MI in the garnet and occurrence of apatite. **(a–b)** Granoblastic texture of garnet (Grt) and clinopyroxene (Cpx) with interstitial plagioclase (Pl). Garnets contain MI in the inner part organized in clusters and indicated by black arrows. **(c)** Apatite (Ap) occurs included in garnet or in the matrix. **(d)** Cluster of MI in parallel polars (sx) and close up in crossed polars (dx) of inclusions where the polycrystalline nature is visible. Mineral abbreviations are from Warr (2021).

last two phases also contain significant amounts of F, e.g., ≤ 0.11 wt %, measured via EMP (Table 2), an element which is often observed to be rather partitioned in biotite instead of other phases, at least in granitic systems. The detection limit for F for the analyses in Table 3 is 0.05 wt %.

4.4 Nanogranitoid re-homogenization experiments and melt composition

Re-homogenization experiments were performed under the conditions expected for the formation of the garnet during the metamorphic peak, 1000 °C and 2.2 GPa (Rötzler et al., 2008). Although in these conditions the inclusions are fully re-homogenized, they also display the formation of a new garnet (more Mg-rich and Ca-poor; Figs. 6a, b and S2 in the Supplement) at the inclusion–host interface. Based on the extensive knowledge derived from previous re-homogenization experiments on similar inclusions (e.g., Bartoli et al., 2013; Ferrero et al., 2018), this microstructural feature is interpreted as evidence of melt–host interaction, possibly due to the fact that the confining P during the experiment was insufficient to stabilize the inclusion–garnet system (see also Ferrero et al., 2021b). Moreover, the presence of corundum needles in one inclusion (Fig. S2 in the Supplement) suggests that the samples were overheated; i.e., the experimental T was higher than the real formation T of the inclusion–host system (Ferrero et al., 2018). Thus, two additional batches of experiments were performed at 2.7 and 3 GPa and 975 °C (see Table S2 in the Supplement), which resulted in fully re-homogenized inclusions without evidence of melt–host interaction (Fig. 6c and d).

The melt is mainly granitic (Fig. 7a–b) with a high alkalis content (on average: $Na_2O + K_2O = 8.21$ wt %; Na_2O / $K_2O = 1.50$ wt %; Table 3). TiO_2 (0.26 wt %), MnO (0.05 wt %) and MgO (0.49 wt %) are generally low, whereas CaO (1.69 wt %) and FeO (1.60 wt %) are slightly higher with a $FeO + MgO + TiO_2$ value of 2.35 wt % and a Mg# of 34. In general, the re-homogenized glasses show a slight variability in some components. In particular, SiO_2 displays an inverse correlation with respect to Al_2O_3, Na_2O and CaO, whereas for K_2O the variability is independent of the SiO_2 content (Fig. 8). $FeO + MgO + TiO_2$ is instead fairly constant (~ 2.3 wt %). The melt is also mainly peraluminous (alumina saturation index (ASI): molar Al_2O_3 / $(Na_2O + K_2O + CaO) = 1.13$) and alkalic to alkali–calcic (Fig. 7c–d). The H_2O content was obtained by the difference between 100 and the totals of the EMPA analyses, and it is on average 4.82 wt %. The Cl concentration was also

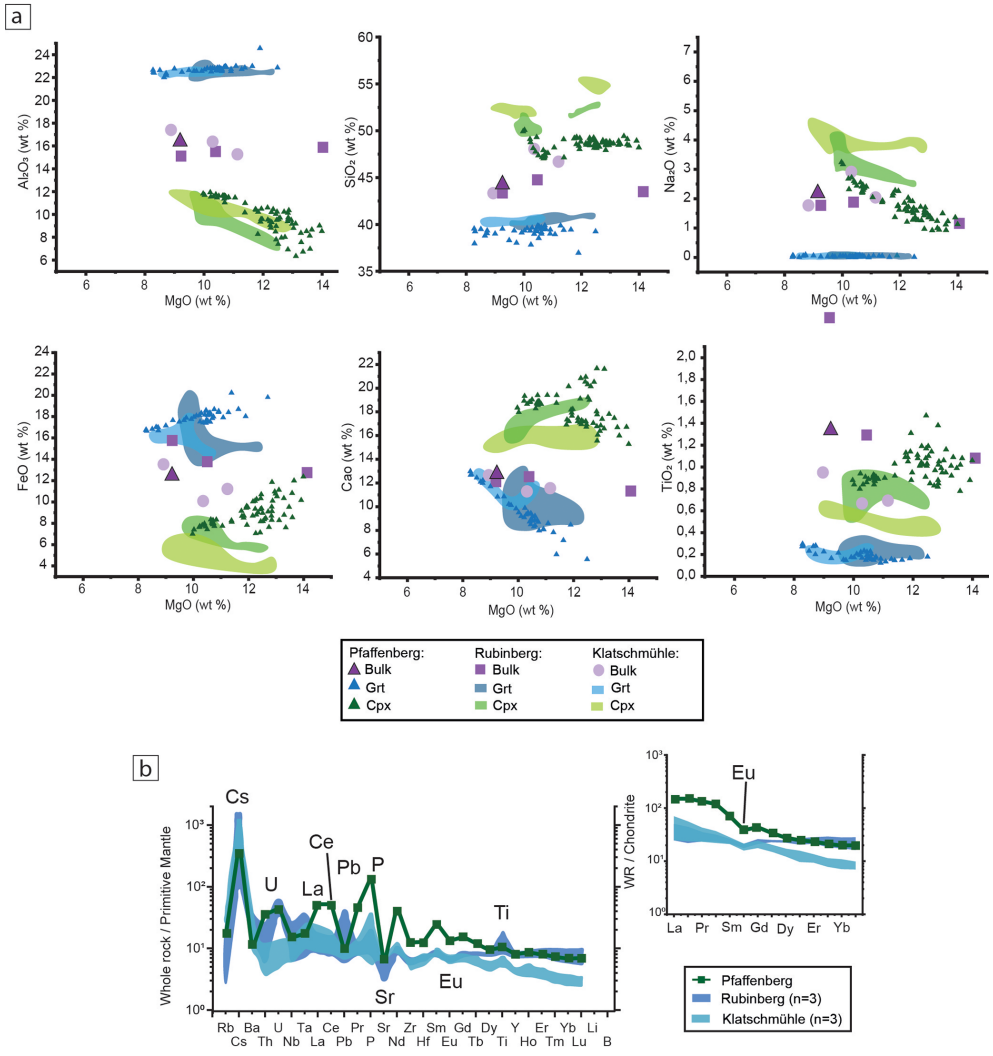

Figure 3. Chemical composition of the bulk and garnet and clinopyroxene of Pfaffenberg eclogites. **(a)** Variation in the major oxides relative to MgO wt % of whole rock, garnet and clinopyroxene. The data are compared to the whole rock and mineral constituent of RUB and KLA eclogites (Borghini et al., 2020). **(b)** Primitive mantle (Sun and McDonough, 1989; McDonough and Sun, 1995) normalized whole-rock trace element pattern of Pfaffenberg eclogites compared to the whole-rock patterns of RUB and KLA eclogites (Borghini et al., 2020).

measured via EMPA, and it is exceptionally high, with an average of 0.41 wt % (Table 3).

The content of F in the melt was calculated (see Methods) considering the partitioning of this element between apatite and melt. The halogen content in apatite was measured via EMPA in apatite grains included in garnet and scattered in the matrix, and both types show similar average F contents (see Table 1), whereas the F content calculated for the melt is 0.23 wt % and 0.24 wt % respectively. The results are reported in Table S3 of the Supplement.

The major element composition of PF melt is close to the MI trapped in the eclogites of RUB and KLA (Borghini et al., 2018, 2020). They are mainly granitic, slightly peraluminous and mainly alkalic (Fig. 7). However, in particular, the melt in PF contains slightly less SiO_2 and Al_2O_3 and slightly more $FeO + MgO + TiO_2$ and CaO (Fig. 8). When compared to the entire dataset of MI in high-grade rocks from Bartoli et al. (2016; green shading in Fig. 8), i.e., over 600 inclusions, the content of $FeO + MgO + TiO_2$ (2.35 wt %) of the melt measured in Pfaffenberg lies within the range of the ∼ 90 % of the inclusions ($FeO + MgO + TiO_2 = \sim 0.25$ wt %–2.5 wt %), whereas CaO content is slightly higher (1.69 wt % in Pfaffenberg vs. < 1.5 wt % in the database; Bartoli et al., 2016; Fig. 8). The melt in PF is also more alkali–calcic than the others (Fig. 7d).

Trace element patterns normalized to primitive mantle show that the melt in Pfaffenberg is enriched in LILE (Cs in particular) Th, U, Li, B, Pb and slightly in LREE (Fig. 9 and Table S4 in the Supplement). The melt is also minimally enriched in Zr, Nd and Hf; it shows a negative anomaly for

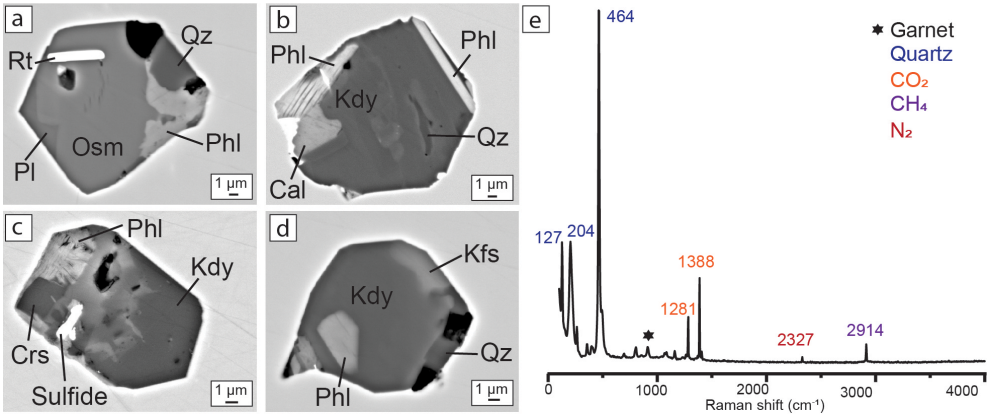

Figure 4. BSE images of nanogranitoids included in garnets from Pfaffenberg eclogites. They show a well-developed negative crystal shape and contain **(a)** quartz (Qz), osumilite (Osm), phlogopite (Phl), plagioclase (Pl) and rutile (Rt); **(b)** Qz, Phl, kumdykolite (Kdy) and calcite (Cal); **(c)** Phl, Kdy, cristobalite (Crs) and sulfide; and **(d)** Phl, Kdy, Qz and K-feldspar (Kfs). **(e)** Occasionally they may also contain a fluid phase with CO_2, CH_4 and N_2.

Nb, Ta and Sr, and it is depleted in Ti. As for the major elements, TEs also show similarities with the melt trapped in the aforementioned eclogites (Borghini et al., 2018, 2020) as well as in the eclogites of Saidenbach (Borghini et al., 2023). Although the patterns of the different melts are overall very similar, in PF the melt is slightly more enriched in Cs and Nd, whereas the melt in Saidenbach shows higher concentrations of Pb, U, Zr and Hf and a depletion of Nb.

When compared with other natural (Stepanov et al., 2016) and experimental (Skora et al., 2015) melts resulting from the partial melting of metasediments under UHP conditions, the melt in the PF eclogite shows similarities in particular with the melt in the UHP ($P > 4.5$ GPa-$T = 1000$ °C) paragneiss of the Kokchetav Massif (Kazakhstan). The melt in the latter case is granitic and peraluminous (ASI ~ 1.2) and, as with the melt in PF, enriched in LILE, Pb, Th and U. However, the PF melt is richer in Cs, whereas the one in the Kokchetav Massif is richer in LREE (Fig. 9). The experimental melts obtained from the partial melting of calcareous marine metasediments at 3 GPa and 1000 °C are significantly different in terms of major elements, as they are granodioritic, metaluminous (ASI ~ 0.6–0.9) and subalkaline (Skora et al., 2015). The comparison in terms of TEs shows similar trends, but the enrichments in the melt in PF are almost 2 orders of magnitude higher, and the experimental melts show positive Sr, Nd and Ti anomalies opposite to what is observed in PF (Fig. 9). The comparison to the bulk continental crust (CC; Rudnick and Gao, 2003), the upper continental crust (UCC; Rudnick and Gao, 2003) and the globally subducting sediments (GLOSS; Plank and Langmuir, 1998) shows that the PF melt shares similar trends in particular for the positive anomaly of LILE, LREE, Th, U, Li and B and negative anomaly of Nb and Ta, although the magnitude of both enrichment and depletion is much higher in PF (Fig. 9).

5 Discussion

5.1 Composition of primary melt and nature of the source rock

The composition of major and trace elements of a melt trapped in primary MI gives important information about the source rock and the phases involved in the partial melting reaction (e.g., Acosta-Vigil et al., 2010, 2012; Ferrero et al., 2018, 2021b; Bartoli et al., 2019). In Pfaffenberg the investigated eclogites contain a hydrous granitic melt high in alkalis. The random distribution of the inclusions indicates that they are primary and are thus trapped during the garnet growth (e.g., Cesare et al., 2015; Ferrero et al., 2018). The presence of feldspar polymorphs – rather than the stable counterparts – in the phase assemblage crystallized in the inclusions suggests that the inclusions are also chemically preserved (Ferrero et al., 2016; Ferrero and Angel, 2018). The relatively high values of $FeO + MgO + TiO_2$ could be related to the production of the melt at temperatures near 1000 °C (Ferrero et al., 2021b). Moreover, their successful re-homogenization under P–T conditions rather close to peak conditions recorded by nearby spinel peridotites, as reported by Schmädicke et al. (2010), is strong evidence that these inclusions have not lost H_2O, as this would have prevented the melt from re-homogenizing in such conditions (e.g., Bartoli et al., 2013, 2016; Ferrero et al., 2018).

In terms of major elements, the melt is similar in composition to silicate melts from melting metasediments trapped in other eclogites (Borghini et al., 2018, 2020, 2023). Moreover, its granitic nature makes it similar to other nanogranitoids from the melting of rocks belonging to the continental crust (e.g., Ferrero et al., 2021a) even if formed at lower P (e.g., Bartoli et al., 2016; Carvalho et al., 2018; Ferri et al., 2020; Gianola et al., 2020; Ferrero et al., 2021a).

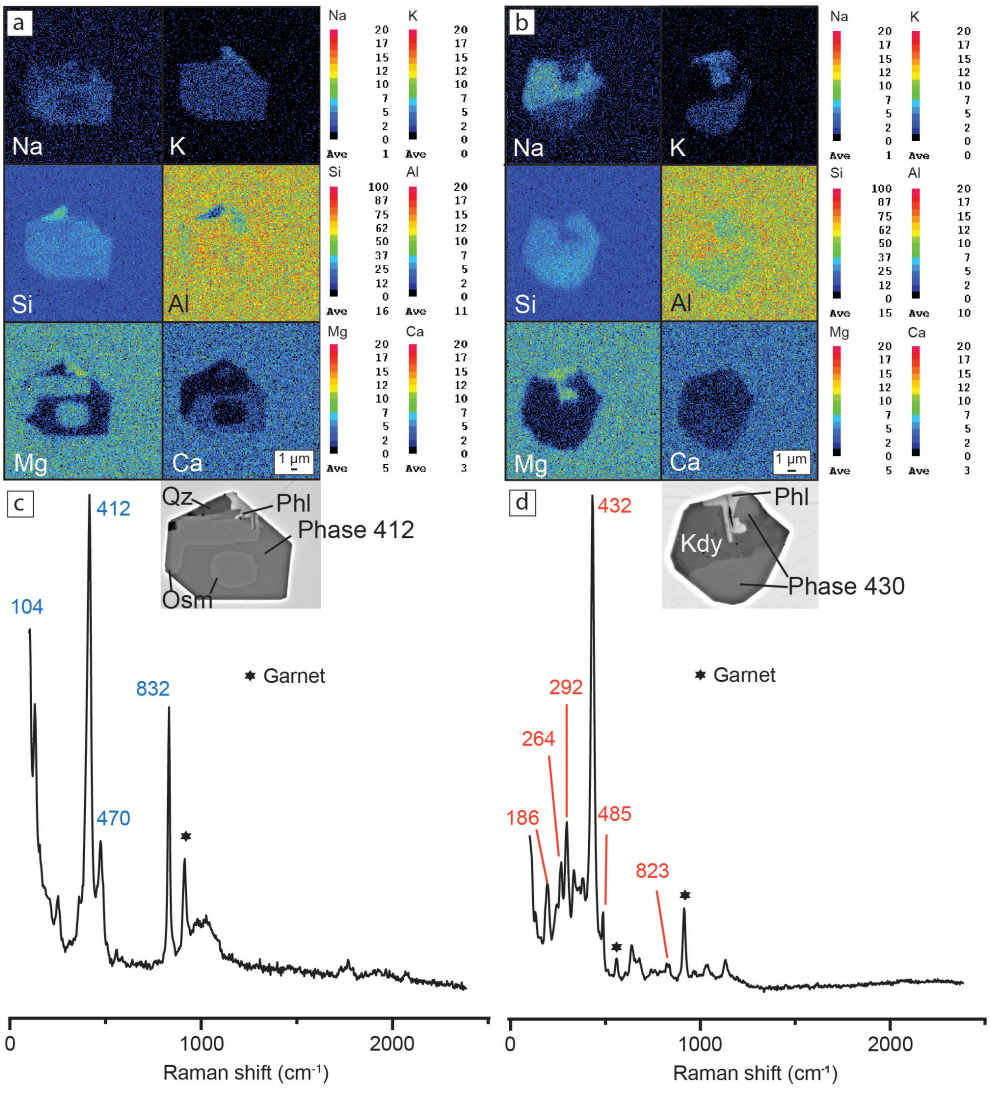

Figure 5. EDS elemental maps of nanogranitoids **(a, b)** and Raman spectra of phase 412 and 430 **(c, d)**.

The melt is enriched in Cs, Pb, Rb, U, Li and B compatible with the involvement of white mica in the melt-producing reaction, as already suggested for the melts in the eclogites of the Granulitgebirge (Borghini et al., 2018, 2020) and Erzgebirge (Borghini et al., 2023) and for similar melts trapped in metasediments of El Hoyazo (Acosta-Vigil et al., 2010; Fig. 9). The TE trends of Pfaffenberg melt composition resemble the granitic melts found in the paragneiss of the Kokchetav Massif (Stepanov et al., 2016) and the continental crust itself, both CC and UCC, and GLOSS – apart from the considerably higher enrichments in Cs, Th and U – thus making it even more likely that the melt source rock was a high-grade felsic rock (Fig. 9). When compared instead with calcareous marine metasediments (Skora et al., 2015), the melt investigated here displays similar trends but a significantly lower order of magnitude for LILE (excluding Ba), Th, U and LREE, besides some clear differences such as positive anomalies in Sr, Nd and Ti. The involvement of white mica, the peraluminous nature of the melt and its similarities with the melt found in the paragneiss of the Kokchetav Massif (Stepanov et al., 2016) suggest that the protolith was most likely of sedimentary origin. The presence of U in the melt is possibly related to the additional contribution of a fluid to the melt-producing reaction (Borghini et al., 2018, 2020), a scenario furthermore supported by the presence of CO_2, CH_4 and locally N_2 in nanogranitoids. The H_2O content is moderate ($\sim$ 5 wt %) and significantly lower than the amount required to saturate the system at 975 °C and $\sim$ 3 GPa (see Johannes and Holtz, 1996), suggesting melting under low a_{H_2O}. Some whole-rock TE enrichments (LREE, Th, U, P and Nb) may also point toward an alternative source rock: an alkali basalt/gabbro (see discussion below).

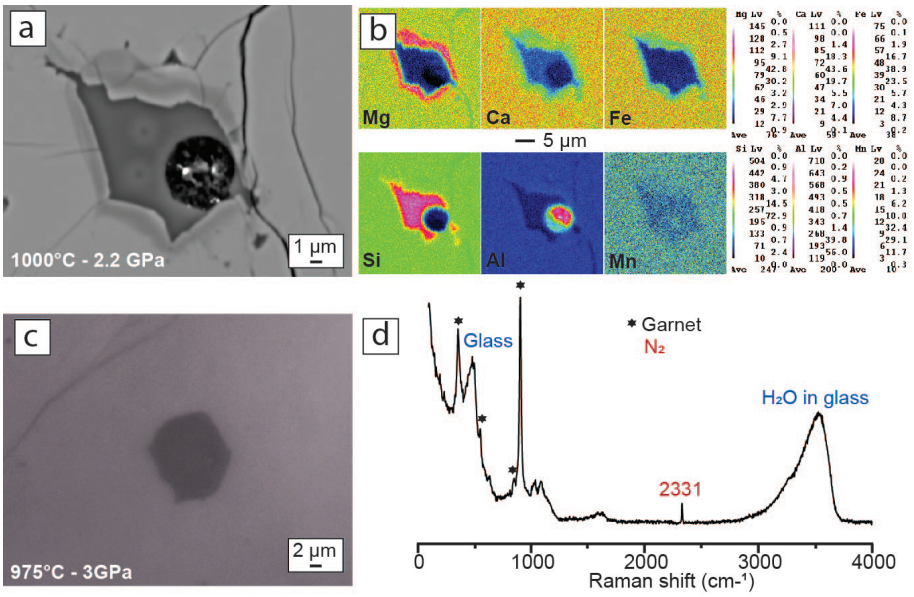

Figure 6. BSE image of re-homogenized inclusions at 1000 °C and 2.2 GPa **(a)** that have reacted with the host garnet, as shown in the elemental map **(b)**; the reaction formed a new garnet with a higher content of Mg and lower content of Ca and Fe. **(c)** Reflected light photomicrograph of a re-homogenized melt inclusion at 975 °C and 3 GPa with a relative Raman spectrum **(d)**. At the present stage of our knowledge, it is unclear if the N_2 peak represents its content in the melt or if it is atmospheric.

5.2 Metasomatizing agent and metasomatism

The eclogite lenses containing a granitic melt reported by Borghini et al. (2018, 2020, 2023) were interpreted as representing a mafic rock that recrystallized at depth, trapping a silicate melt derived externally, i.e., generated from melting at depth of surrounding metasediments. As already stated, these previous findings share crucial similarities with the Pfaffenberg case investigated in this contribution, i.e., the same host rocks and very similar melt composition (both as major and traces). Hence, it is likely that at Pfaffenberg we also see an occurrence of a melt, which, after originating in the surrounding subducted continental crust, interacted with a pre-existing mafic layer in the peridotite body, causing its recrystallization with garnet formation, which in turn led to the entrapment of the melt itself as primary MI (Borghini et al., 2020) (see Sect. 5.3).

Yet, if the possibility of an alkali basalt/gabbro as a protolith is taken into account, the possibility of melt genesis via partial melting should be discussed further. Under the *P*–*T* conditions experienced by the Pfaffenberg samples, the alkali gabbro/basalt would have most likely been a phengite-bearing eclogite. Experimental partial melting of a mafic protolith under HT and HP conditions generally produces a tonalitic to trondhjemitic melt (e.g., Beard and Lofgren, 1991; Laurie and Stevens, 2012; Rapp et al., 1991; Rapp and Watson, 1995). In some limited cases, the melt is granodioritic (Schmidt et al., 2004) and, for small degrees of partial melting, also granitic (Rapp et al., 1991; Skjerlie and Patiño Douce, 2002). In most of the experiments, phengite is not present, and in the cases of mafic protolith with more K where phengite is present, the partial melting of phengite-bearing eclogite produces peritectic garnet (Schmidt et al., 2004; Skjerlie and Patiño Douce, 2002) and kyanite (Skjerlie and Patiño Douce, 2002). In modal amounts, the partial melting reactions involving phengite would produce a relatively small volume of both melt and new peritectic garnet, with phases such as garnet and clinopyroxene predating the partial melting still being preserved because they are not consumed during the melting reaction. The Pfaffenberg samples only display inclusions in the inner part of the garnets and not in its mantle, as would be expected in the case of a new peritectic garnet growing on a pre-melting garnet. Moreover, this melt, as discussed above, is very similar in terms of major and trace elements to other melts produced by the partial melting of metasediments (Figs. 7, 8 and 9; Borghini et al., 2018, 2020, 2023) and to the trace element signature of the continental crust itself (Fig. 9). For a detailed discussion on the microstructural and microchemical criteria used to rule out partial melting of a previous protolith, the reader is referred to Borghini et al. (2020).

Since we rule out the partial melting scenario, as discussed above, the melt preserved in the crystallized MI likely represents a metasomatizing agent. The crystallized MI in PF have a clear granitic composition, with a constant mineral assemblage comprising feldspars, quartz and micas, and lack any evidence of system reopening, e.g., decrepitation cracks. Polycrystalline inclusions (also called multiphase solid inclusions or MSI) have already been reported in

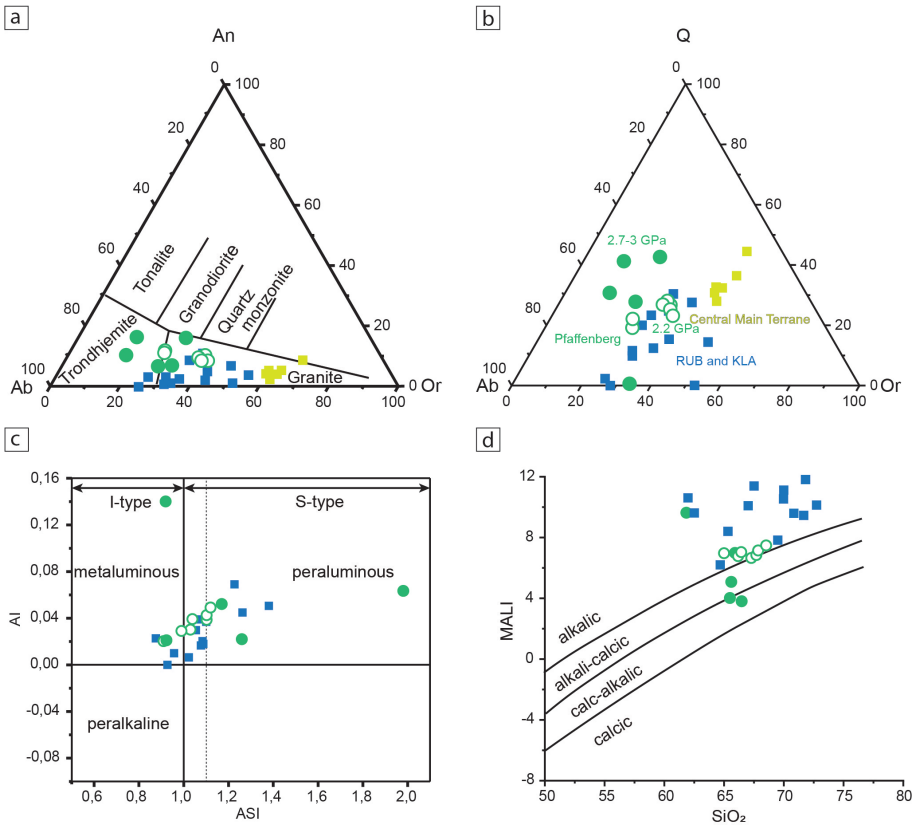

Figure 7. CIPW normative anorthite–orthoclase–albite (An–Or–Ab) **(a)** and quartz–orthoclase–albite (Q–Or–Ab) **(b)** diagrams showing the major element composition of the melt measured in the eclogites of Pfaffenberg compared with the melt in the RUB and KLA eclogites (1000 °C, 2.2 GPa; Borghini et al., 2018) and the melt in the HP metasediments of the Central Main Terrane (1050 °C, 2 GPa; Ferrero et al., 2021b). **(c)** Plot of the aluminum saturation index (ASI = molar Al_2O_3 / ($CaO + Na_2O + K_2O$)) vs. the alkalinity index (AI = molar Al_2O_3-(Na_2O+K_2O); see Frost and Frost, 2008) of the melt in the PF eclogites. **(d)** Diagram SiO_2 (wt %) vs. modified alkali–lime index (MALI = $Na_2O + K_2O$-CaO); see Frost and Frost (2008). In both diagrams the melts in RUB and KLA are plotted for comparison. The fields in **(a)**, **(c)** and **(d)** and the dotted line in **(c)** are from Bartoli et al. (2016).

HP/UHP rock types and are interpreted as containing metasomatizing agents: garnet pyroxenites (Malaspina et al., 2006, 2009; Zelinkova et al., 2023), orogenic garnet peridotites (Malaspina et al., 2009; Čopjaková and Kotková, 2018; Naemura et al., 2018), spinel-bearing harzburgite xenoliths (Schiano et al., 1995), eclogites (Faryad et al., 2013; Gao et al., 2012, 2013, 2014; Chen et al., 2014; Liu et al., 2018) and paragneisses (Stepanov et al., 2016). However, MSI are generally rather different in phase assemblage with respect to the MI in Pfaffenberg. For example, some MSI contain mostly hydrous phases (e.g., Malaspina et al., 2006, 2009) or mainly phyllosilicates, phosphate and carbonates (Naemura et al., 2018; Zelinkova et al., 2023), and others are completely devoid of OH-bearing phases (e.g., Gao et al., 2012, 2013, 2014; Chen et al., 2014; Liu et al., 2018) or contain glass, sulfides and mafic minerals (Schiano et al., 1995). Moreover, the MSI reported in the literature often show decrepitation features, such as irregular shape, protrusion textures, radial cracks surrounding the inclusions and healed cracks in the host mineral (e.g., Chen et al., 2014; Gao et al., 2014; Liu et al., 2018; Brown, 2023), which suggests that they are not fully preserved due to material loss (or gain) via system reopening after entrapment. For a more detailed comparison pertaining to this type of inclusion, the reader is referred to Borghini et al. (2020, 2023).

Another term of comparison for the metasomatizing agent found in Pfaffenberg is provided by the extremely vast literature on xenoliths of either mantle (e.g., Liptai et al., 2021; Andersen et al., 1984; Wulff-Pedersen et al., 1996; Sajona et al., 2000; Bali et al., 2002) or crustal origin (e.g., Németh et al., 2021; Dallai et al., 2022), found mostly in basaltic magmas. Melt-like metasomatizing agents are reported in xenoliths to be either silicic (e.g., Schiano et al., 1995; Liptai et al., 2021; Németh et al., 2021; Dallai et al., 2022) or carbonatitic (Guzmics et al., 2008) in composition and are found as crystallized (e.g., Guzmics et al., 2008; Liptai et al., 2021) or glassy MI (e.g., Schiano et al., 1995; Golovin and Sharygin, 2007; Németh et al., 2021; Dallai et al., 2022) or even melt pockets (Bali et al., 2002). However, in the case studies mentioned above, the metasomatizing agent is interpreted as

Table 2. EMP analyses of mineral phases in nanogranitoids.

Phase	Kumdykolite					Osumilite			Biotite		Clinopyroxene	Phase 412	Phase 430	Chlorite	Amphibole
Sample name	PF5.1-s2 -G1-i04	PF5.2-s2 -G2-i04	PF5.2-s1 -G1-i01	PF5.2-s1 -G1-i04	PF5.2-s1 -G1-i07	PF5.2-s2 -G1-i09	PF5.1-s2 -G1-i01	PF5.1-s2 -G2-i07	PF5.1-s2 -G2-i07	PF5.1-s1 -G2-i23	PF5.2-s1 -G1-i01	PF5.2-s1 -G2-i03	PF5.2-s1 -G1-i10	PF5.1-s2 -G1-i09	PF5.1-s1 -G2-i11	PF5.1-s1 -G2-i24
wt %																
SiO_2	71.23	63.68	67.87	70.22	73.89	66.32	59.34	59.53	57.76	38.10	36.64	52.10	68.65	72.16	37.90	40.52
TiO_2	0.00	0.05	0.04	0.02	0.07	0.00	0.06	0.06	0.07	3.84	2.06	0.23	0.02	0.03	0.01	1.18
Al_2O_3	19.12	22.29	20.89	21.55	17.87	22.12	22.66	21.41	22.77	18.46	17.00	12.07	20.64	16.34	15.53	19.50
Cr_2O_3	0.01	0.00	0.00	0.00	0.04	0.03	0.00	0.00	0.02	0.05	0.00	0.00	0.00	0.00	0.00	0.00
Fe_2O_3	0.00	0.00	0.00	0.00	0.00	0.00	0.00	0.00	0.00	0.00	0.00	0.00	0.00	0.00	0.00	0.00
FeO	0.62	1.16	0.67	0.60	0.59	0.64	4.07	4.21	4.05	6.73	19.78	4.05	0.95	0.66	10.15	8.38
MnO	0.00	0.03	0.06	0.02	0.00	0.00	0.00	0.07	0.05	0.04	0.06	0.00	0.00	0.00	0.28	0.01
MgO	0.02	0.26	0.05	0.04	0.06	0.03	8.43	8.84	8.33	18.98	11.22	10.40	0.30	0.04	24.37	14.47
CaO	1.51	4.27	2.98	2.13	1.89	2.93	0.17	0.23	0.25	0.30	1.26	17.21	2.03	1.58	0.26	11.22
Na_2O	6.24	7.43	5.54	2.70	3.92	5.34	1.68	1.57	1.77	0.48	0.07	4.35	3.06	0.81	0.45	2.32
K_2O	0.19	0.08	0.18	0.20	0.10	0.04	3.95	4.13	4.24	9.26	9.38	0.02	2.96	3.81	0.09	0.81
P_2O_5	0.02	0.00	0.02	0.00	0.00	0.00	0.03	0.01	0.00	0.02	0.03	0.03	0.01	0.00	0.00	0.03
F	0.01	0.00	0.00	0.00	0.00	0.01	0.00	0.00	0.00	0.00	0.00	0.00	0.11	0.07	0.00	0.00
Total	98.97	99.25	98.30	97.48	98.43	97.46	100.39	100.06	99.31	96.26	97.5	100.46	98.73	95.50	89.04	98.44

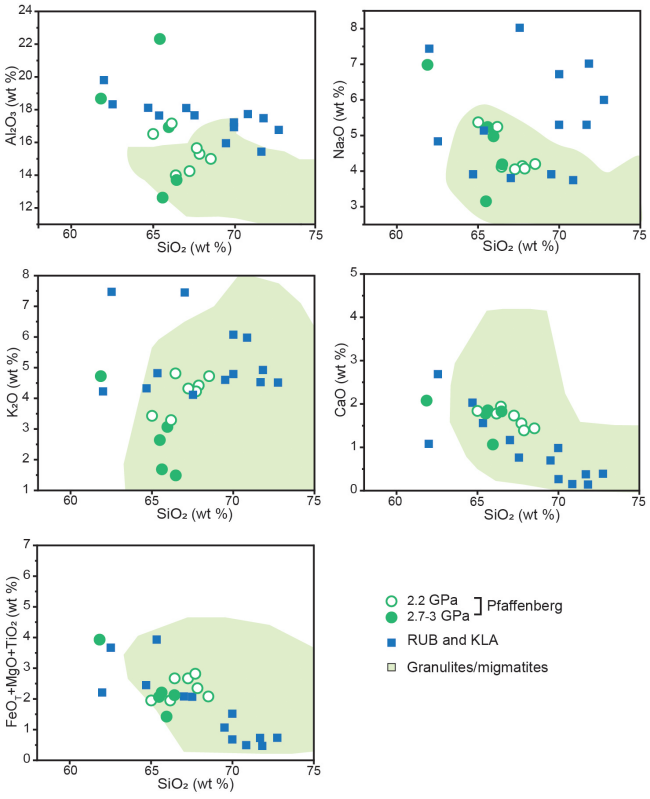

Figure 8. Variation diagram of major oxides relative to SiO_2 wt % of the melt in re-homogenized nanogranitoids in Pfaffenberg eclogites and in glassy and re-homogenized nanogranitoids in RUB and KLA eclogites. The green shading is melt inclusions measured in granulites/migmatites present in the dataset from Bartoli et al. (2016).

being the product of partial melting of either the mantle itself or the subducted oceanic crust, in some cases with a minor contribution from both metasediments and metabasalts. Only one case study suggests the involvement of the continental crust, but the authors proposed that crustal material from a previous subduction was stored in the lithospheric mantle and melted during decompression (Dallai et al., 2022). This is not the case for the melt in Pfaffenberg because the geochemical features of the melt can be ascribed entirely and exclusively to the re-melting of continental crust in peak conditions during the subduction of the crust at mantle depth.

5.3 Nature and origin of the host rock

Rocks similar to those at Pfaffenberg, i.e., garnet- and pyroxene-bearing rocks, crop out throughout the entire Saxothuringian Zone and were for a long time classified as garnet pyroxenites (see discussion in Borghini et al., 2020). However, all the chemical features of the rocks investigated at Pfaffenberg are more typical of eclogites than of garnet pyroxenites (Borghini et al., 2020, and references therein). In fact, the Pfaffenberg samples contain $Na_2O > 2$ wt %; a

Table 3. Melt major element composition and P–T conditions used to perform nanogranitoid re-homogenization experiments.

Name	PF1a	PF1b	PF2	PF3	PF4	PF5a	PF5b	27C	12DC	23C	24C	15DC	Average	SD
Duration (h)	24	24	24	24	24	24	24	24	24	24	24	24		
T (°C)	1000	1000	1000	1000	1000	1000	1000	975	975	975	975	975		
P (GPa)	2.2	2.2	2.2	2.2	2.2	2.2	2.2	2.7	2.7	3	3	3		
wt %														
SiO_2	68.52	67.85	66.45	67.27	67.70	66.18	65.01	65.95	66.49	65.62	65.49	61.86	66.20	2.59
TiO_2	0.30	0.20	0.34	0.46	0.32	0.24	0.30	0.21	0.05	0.33	0.18	0.23	0.26	0.09
Al_2O_3	15.09	15.36	14.07	14.30	15.70	17.20	16.53	16.93	13.76	12.69	22.34	18.72	16.06	2.54
FeO	1.54	1.77	1.75	1.73	1.83	1.35	1.38	0.92	1.58	1.39	1.22	2.72	1.60	0.85
MnO	0.05	0.05	0.02	0.04	0.04	0.05	0.05	0.00	0.04	0.05	0.00	0.16	0.05	0.04
MgO	0.24	0.38	0.57	0.48	0.67	0.36	0.27	0.29	0.52	0.49	0.66	0.97	0.49	0.43
CaO	1.44	1.39	1.94	1.73	1.56	1.78	1.84	1.07	1.84	1.85	1.78	2.08	1.69	0.76
Na_2O	4.19	4.07	4.12	4.04	4.14	5.24	5.37	4.98	4.17	5.24	3.15	6.96	4.64	1.04
K_2O	4.72	4.42	4.82	4.33	4.26	3.29	3.43	3.07	1.48	1.69	2.64	4.72	3.57	1.30
P_2O_5	0.00	0.15	0.63	0.49	0.23	0.16	0.09	0.22	0.11	0.21	0.10	0.22	0.22	0.16
Cl	0.55	0.49	0.58	0.60	0.56	0.42	0.38	0.15	0.34	0.49	0.15	0.23	0.41	0.17
Total	96.64	96.13	95.29	95.47	97.01	96.27	94.65	93.79	90.36	90.03	97.71	98.86	95.18	
Q	22	23	20	23	22	18	16	23	31	24	32	0	21	
Or	28	26	28	26	25	19	20	18	9	10	16	28	21	
Ab	35	34	35	34	35	44	45	42	35	44	27	54	39	
An	7	6	6	5	6	8	9	4	8	6	8	6	7	
ASI	1.03	1.10	0.91	0.99	1.10	1.12	1.04	1.26	1.17	0.92	1.98	0.92	1.13	
H_2O by diff	3.36	3.87	4.71	4.53	2.99	3.73	5.35	6.21	9.64	9.97	2.29	1.14	4.82	
CaO/Al_2O_3	0.10	0.09	0.14	0.12	0.10	0.10	0.11	0.06	0.13	0.15	0.08	0.11	0.11	
$Na_2O + K_2O$	8.91	8.49	8.94	8.37	8.40	8.53	8.80	8.04	5.64	6.92	5.79	11.68	8.21	
Na_2O/K_2O	0.89	0.92	0.85	0.93	0.97	1.59	1.57	1.62	2.82	3.10	1.19	1.47	1.50	
Mg#	21	27	37	32	39	31	25	36	36	38	49	38	34	
MALI	7.47	7.10	7.00	6.64	6.84	6.75	6.96	6.98	3.80	5.07	4.01	9.61	6.52	
AI	0.03	0.04	0.02	0.03	0.04	0.05	0.04	0.02	0.05	0.14	0.06	0.02	0.05	
$FeO + MgO + TiO_2$	2.08	2.35	2.66	2.67	2.82	1.95	1.95	1.42	2.15	2.21	2.06	3.93	2.35	
$FeO + MgO$	1.78	2.15	2.32	2.21	2.50	1.71	1.65	1.21	2.10	1.87	1.89	3.69	2.09	

TiO_2 content of ~ 1 wt %, which is higher than the content of Cr_2O_3 and Ni that are respectively 300 and 31 ppm; and a Mg# of 57 – features that are all more compatible with an eclogite than a pyroxenite (see Svojtka et al., 2016; Borghini et al., 2020). Clinopyroxene shows a variable Jd content, with the highest Jd values observed in clinopyroxenes included in garnet, i.e., 20 mol % on average. Clinopyroxenes in the matrix show a lower Jd concentration, possibly due to diffusion of Na_2O in the symplectites surrounding them or in the exsolution in the core. In terms of TEs, the rock shows a subduction-related signature with the enrichment in LILE (Cs in particular), Th and U; the Pb enrichment is similar to the eclogites of Klatschmühle, whereas the Ti content is more akin to the eclogites in Rubinberg (Fig. 3).

One feature unique to Pfaffenberg is the strong enrichment in LREE and P (Fig. 3b). This cannot simply be attributed to the interaction with the infiltrating melt, whose composition is very close to the melts in Rubinberg and Klatschmühle (Fig. 9). The prevalent enrichment of P and LREE in Pfaffenberg eclogites thus most likely reflects a difference in the protolith. The main carriers of P and LREE in mafic rocks are apatite and allanite (Hermann, 2002; Spear and Pyle, 2002). In this case, apatite was possibly already present in the mafic protolith, and it recrystallized during the metasomatic reaction. The LREE were most likely redistributed and stored in the clinopyroxene, whereas the P and the availability of CaO led to an increase in the apatite mode. The presence of heterogeneous layers within the same peridotite body is not surprising, and in the literature several examples of lenses with very variable compositions have been reported (e.g., Ronda: Bodinier et al., 2008; Lherz: Bodinier et al., 1990; and External Ligurides: Borghini et al., 2016).

Thus, based on the bulk rock composition and the absence of the TE signature of the melt in the host rock, we propose that the protolith was a mafic level rich in FeO and CaO, likely garnet-free and already containing apatite. The successful re-homogenization of the nanogranitoids at 2.7–3 GPa adds another important piece of information. Instead of the 2.2 GPa proposed for the other two cases of MI-bearing eclogites in the Granulitgebirge (Borghini et al., 2020), at Pfaffenberg anatexis of the surrounding metasediments and melt–rock interaction (metasomatism) took place

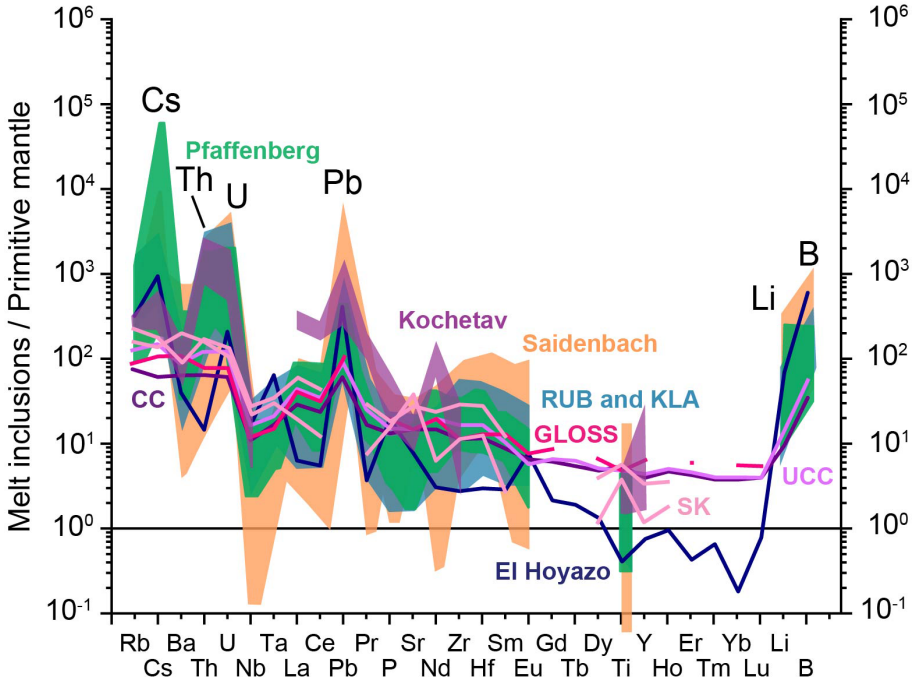

Figure 9. Primitive mantle (Sun and McDonough, 1989; McDonough and Sun, 1995) normalized trace element analyses of the melt in the eclogites from Pfaffenberg ($n = 56$, this study; see Table S4 in the Supplement) compared with trace elements of the melt in eclogites from RUB and KLA (Borghini et al., 2020) and Saidenbach in the Erzgebirge (Borghini et al., 2023), melt in the metasediments of El Hoyazo in Spain (Acosta-Vigil et al., 2010), melt from experiments of the partial melting of calcareous marine sediments (SK; experiment runs at 3 GPa and 1000 °C; Skora et al., 2015), and melt in the paragneiss of the Kokchetav Massif in Kazakhstan (Stepanov et al., 2016) and the trace element composition of the bulk continental crust (CC; Rudnick and Gao, 2003), the upper continental crust (UCC; Rudnick and Gao, 2003) and the globally subducting sediments (GLOSS; Plank and Langmuir, 1998).

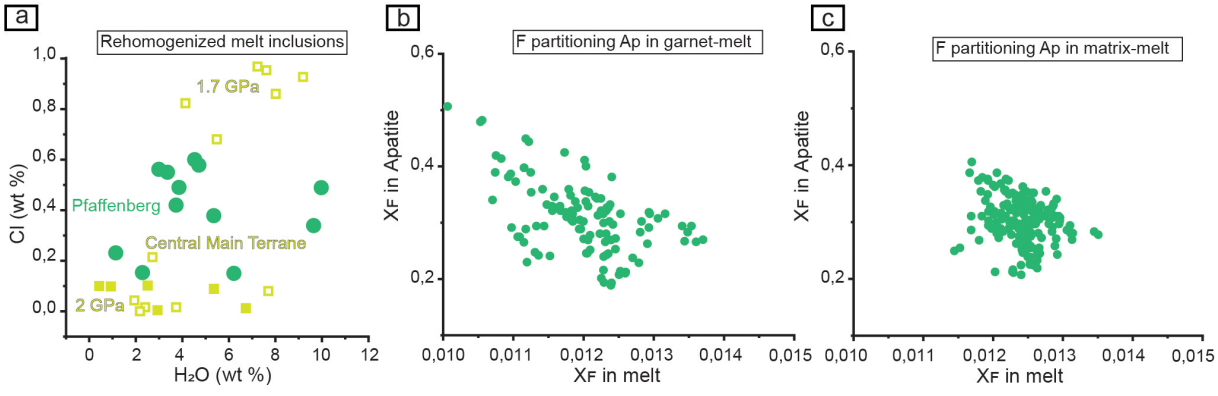

Figure 10. Volatile content of the melt in Pfaffenberg. **(a)** Contents of Cl and H_2O measured on the re-homogenized MI compared to the melt in the HP metasediments of the Central Main Terrane (Ferrero et al., 2021b). Molar fraction of F in the melt calculated based on the partitioning of this element between apatite and melt for both apatite in the garnet and melt **(b)** and apatite in the matrix and melt **(c)**.

in/near UHP conditions, very close to the boundary between the quartz and coesite fields (Bose and Ganguly, 1995). Partial melting at similar P and slightly lower T (875 °C versus 975 °C) has already been reported in the Bohemian Massif for the HP leucogranulites of the Orlica–Śnieżnik Dome (Saxonthuringian Zone, Bohemian Massif; Ferrero et al., 2015). In the latter the authors excluded decompressional melting as a mechanism for melt production, instead suggesting melting in, or near, peak metamorphic conditions (Ferrero et al., 2015, 2018). Interestingly, similar P–T conditions, 990–1000 °C and 2.6 GPa (Schmädicke et al., 2010) were also proposed for keliphitic spinel peridotites cropping out in Waldheim, close to the samples of this study. In summary, Pfaffenberg represents an additional locality in which

MI-bearing eclogites record a metasomatizing agent that has interacted with the mantle during the subduction of the continental crust at mantle depth – likely at the metamorphic peak during the Variscan orogeny, similarly to what was found in three other localities in the Bohemian Massif (Borghini et al., 2018, 2020, 2023).

5.4 Halogen enrichment in melt and apatite

The presence and mobilization of halogen-rich fluids in subduction zones have been attracting the attention of the scientific community for more than a decade (e.g., John et al., 2012; Pagé et al., 2016; Barnes et al., 2018; Hughes et al., 2018). Halogen-rich fluids and melts are important carriers of Th, U, REE, P and metals (e.g., Antignano and Manning, 2008; Aranovich et al., 2013; Harlov and Aranovich, 2018), and they can influence the stability of OH-bearing mineral phases (e.g., biotite/phlogopite), thus favoring melting at extremely high temperatures (Aranovich et al., 2013; Ferrero et al., 2021b). Halogens are very incompatible elements and are thus generally partitioned in fluids and melts (Barnes et al., 2018). In subduction zones their main carriers are OH-bearing phases, such as amphibole, micas and apatite (Pagé et al., 2016; Harlov and Aranovich, 2018).

Primary MI preserve their original volatile content (Ferrero et al., 2023) and could therefore provide important insights into the fluid regime at the moment of melt entrapment (Carvalho et al., 2018), i.e., in the present case, when the garnet was growing in the presence of melt at mantle depths during the metamorphic peak. Chlorine measured in re-homogenized primary nanogranitoids displays an average of 0.41 wt % (Table 3). When compared with the data available in the literature, such a Cl content is exceptionally high, comparable to both experimental granitic melts coexisting with brines ($\sim$ 0.17 wt %–0.71 wt %, Aranovich et al., 2013; $\sim$ 0.24 wt %–1.63 wt %, Safonov et al., 2014) and natural anatectic melt in HP metapelites ($\leq$ 0.97 wt %, Ferrero et al., 2021b) (Fig. 10). The F content of the melt was instead calculated using the equation of Li and Hermann (2017), which takes into account its non-linear partitioning between apatite and melt. Fluorine was measured by EMP on apatite grains both included in the garnet and present in the matrix, and the average calculated XF in the melt is 0.012, which corresponds to concentrations of 0.23 wt % using apatites included in the garnet and 0.24 wt % with apatite in the matrix. These values are only slightly lower than what was measured in the melt trapped in the HP metasediments of the Central Main Terrane ($\sim$ 3200 ppm or 0.32 wt % on average; Ferrero et al., 2021b). Fluorine is present in lower amounts with respect to Cl, possibly because it tends to be retained/fractionated more easily than Cl in the structure of minerals (Pagé et al., 2016; Hanley and Koga, 2018; Urann et al., 2020).

The high concentration of halogens in the melt points toward the involvement of either a halogen-bearing phase such as a mica or a brine in the melt-producing reaction (Aranovich et al., 2014; Ferrero et al., 2021b). Phengite played a key role in the partial melting reaction based on the melt trace element signature (see above). This phase can contain a significant amount of halogens (Pagé et al., 2016; Urann et al., 2020), and, indeed, in continental rocks equilibrated under eclogite facies conditions, it represents an important sink for these volatile species (Svensen et al., 2001). Interestingly, halogens are far more abundant in MI from Pfaffenberg eclogites than from RUB eclogites (0.10 wt % Cl via EMP analyses; see Ferrero et al., 2023; halogens were not measured in KLA eclogites), despite the fact that in both case studies the trapped melt is an infiltrated metasomatizing melt. One possibility is that the source of the melt now trapped in the eclogites investigated here was different with respect to that of KLA and RUB, maybe a halogen-rich metasediment – however, there is no direct evidence in support of this hypothesis as no such rocks are reported in the area. An alternative possibility is that at Pfaffenberg, in contrast to Rubinberg and Klatschmühle, partial melting of metasediments involved an halogen-rich fluid, i.e., a brine, in agreement with the correspondence between Cl enrichment in the measured re-homogenized MI and melts generated in the presence of brines, especially when the values measured by Aranovich et al. (2013) are considered (see above). This would explain not only the high concentration of halogens in the melt, but also the difference between the melt in Pfaffenberg and Rubinberg. An additional possibility to be entertained is that the mafic layer representing the protolith/precursor of the Pfaffenberg eclogites was already enriched in halogens, which were then redistributed into the infiltrating silicate melt during the metasomatic interaction (e.g., Kendrick et al., 2012). However, this would imply a precursor rock already previously metasomatized by some fluid/brines enriched in halogens (see, e.g., Kobayashi et al., 2019; Hughes et al., 2021) before the melt-related metasomatism recorded by the MI in the peak garnet. Although not an unrealistic scenario, the lack of any traces of the original phase assemblage of the precursor rock prevents the possibility of retrieving information on that stage of the rock evolution.

A further noteworthy aspect is related to the F partitioning inside the nanogranitoids. Commonly expected to be concentrated in biotite (e.g., Ferrero et al., 2021), within the Pfaffenberg nanogranitoids instead are phase 412 and phase 430 (see Sect. 4.3 for more details on these phases), displaying F amounts up to 0.11 wt % (measured via EMP; see Table 2). Such behavior warrants further investigation on F partitioning in a granitic melt hosted in a micrometer-sized closed system such as these inclusions.

6 Conclusions

Melt inclusions are time capsules that are not only useful for collecting information about the major and trace element composition of the melt itself, but also fundamental to

quantifying volatile concentrations at the time of entrapment. The eclogites from Pfaffenberg contain primary MI with a granitic composition and a continental crust origin. Based on microstructural and geochemical data, we argue that the melt trapped in Pfaffenberg eclogites is the metasomatizing agent responsible for the transfer of crustal material in the mantle during the subduction of the continental crust at mantle depths. The interaction of a crustal melt with the mantle is also the process responsible for the formation of the garnet-bearing rocks that we investigate here, i.e., Pfaffenberg eclogites. Moreover, in this case study the halogen-rich composition of the melt suggests that brines were involved in melt production in the source rock, prior to the metasomatic reaction between the eclogite precursor and infiltrating melt itself.

The finding of very similar metasomatizing melts from different localities, as well as of similar trace element signatures in different metasomatic products (mafic and ultramafic rocks) in the Bohemian Massif, suggests that the melt originated from the continental crust was responsible for the contamination of a wide portion of the mantle underneath the orogen. Future work will focus on supporting this hypothesis by targeting the Gföhl Unit in the Moldanubian Zone, where similar associations of rocks, i.e., granulites trapping garnet peridotite bodies with eclogite lenses, have already been identified.

Finally, eclogite lenses in peridotites are not a rare finding in continent–continent collision settings worldwide. It is our opinion that their re-investigation with a keen eye on inclusions will lead to the discovery of further cases of MI-bearing eclogites in other high-temperature HP/UHP orogens in the near future (e.g., Kokchetav Massif, Dabie–Sulu), thus further clarifying how crust–mantle interaction and element recycling occur in the deepest roots of the orogens.

Data availability. The relevant data necessary to evaluate the outcomes can be found either in the paper (Tables 1, 2 and 3) or in the Supplement (Tables S1, S2, S3 and S4). Raw data can be provided by the corresponding author.

Supplement. The supplement related to this article is available online at: https://doi.org/10.5194/ejm-36-279-2024-supplement.

Author contributions. AB, SF and PJO'B designed the project and collected the samples; RF, AB and KG conducted the petrographic study with the help of SF. RF performed trace element analyses in collaboration with PT, and BW performed the re-homogenization experiments in collaboration with RF and AB. AB designed the figures with the help of SF. All authors participated in extensive discussions on data evaluation and interpretation as well as the preparation of the paper.

Competing interests. The contact author has declared that none of the authors has any competing interests.

Disclaimer. Publisher's note: Copernicus Publications remains neutral with regard to jurisdictional claims made in the text, published maps, institutional affiliations, or any other geographical representation in this paper. While Copernicus Publications makes every effort to include appropriate place names, the final responsibility lies with the authors.

Special issue statement. This article is part of the special issue "Probing the Earth: Melt and solid inclusions as probes to understand nature". It is not associated with a conference.

Acknowledgements. We thank Franziska Wilke and Christina Günter for their help during the analyses and Christine Fischer for sample preparation. We thank the German Federal Ministry for Education and Research and the Deutsche Forschungsgemeinschaft (projects FE 1527/2-1, FE 1527/2-2 and FE 1527/4-1 awarded to Silvio Ferrero). This research is part of the project No. 2021/43/P/ST10/03202 co-funded by the National Science Centre (Poland) and the European Union Framework Programme for Research and Innovation Horizon 2020 under the Marie Skłodowska-Curie grant agreement No. 945339. For the purpose of Open Access, the author has applied a CC-BY public copyright licence to any Author Accepted Manuscript (AAM) version arising from this submission. We are thankful to Jörg Hermann and Simona Ferrando for their thorough reviews, which improved the clarity of our paper.

Financial support. This research has been supported by the Deutsche Forschungsgemeinschaft (project nos. FE 1527/2-1, FE 1527/2-2 and FE 1527/4-1) and the European Union Framework Programme for Research and Innovation Horizon 2020 under a Marie Skłodowska-Curie grant agreement (project no. 2021/43/P/ST10/03202, grant no. 945339).

Review statement. This paper was edited by Ross Angel and reviewed by Jörg Hermann and Simona Ferrando.

References

Acosta-Vigil, A., Buick, I., Hermann, J., Cesare, B., Rubatto, D., London, D., and Morgan VI, G. B.: Mechanisms of crustal anatexis: A geochemical study of partially melted metapelitic enclaves and host dacite, SE Spain, J. Petrol., 51, 785–821, https://doi.org/10.1093/petrology/egp095, 2010.

Acosta-Vigil, A., Buick, I., Cesare, B., London, D., and Morgan, G. B.: The extent of equilibration between melt and residuum during regional anatexis and its implications for differentiation of the continental crust: A study of partially melted metapelitic enclaves, J. Petrol., 53, 1319–1356, https://doi.org/10.1093/petrology/egs018, 2012.

Andersen, T., O'Reilly, S. Y., and Griffin, W. L.: The trapped fluid phase in upper mantle xenoliths from Victoria, Australia: implications for mantle metasomatism, Contrib. Mineral. Petr., 88, 72–85, https://doi.org/10.1007/BF00371413, 1984.

Antignano, A. and Manning, C. E.: Fluorapatite solubility in H_2O and H_2O-NaCl at 700 to 900 °C and 0.7 to 2.0 GPa, Chem. Geol., 251, 112–119, https://doi.org/10.1016/j.chemgeo.2008.03.001, 2008.

Aranovich, L. Y., Newton, R. C., and Manning, C. E.: Brine-assisted anatexis: Experimental melting in the system haplogranite-H_2O-NaCl-KCl at deep-crustal conditions, Earth Planet. Sc. Lett., 374, 111–120, https://doi.org/10.1016/j.epsl.2013.05.027, 2013.

Aranovich, L. Y., Makhluf, A. R., Manning, C. E., and Newton, R. C.: Dehydration melting and the relationship between granites and granulites, Precambrian Res., 253, 26–37, https://doi.org/10.1016/j.precamres.2014.07.004, 2014.

Bali, E., Szabó, C., Vaselli, O., and Török, K.: Significance of silicate melt pockets in upper mantle xenoliths from the Bakony – Balaton Highland Volcanic Field, Western Hungary, Lithos, 61, 79–102, https://doi.org/10.1016/S0024-4937(01)00075-5, 2002.

Barnes, J. D., Manning, C. E., Scambelluri, M., and Selverstone, J.: The behaviour of halogens during subduction-zone processes, Springer Geochemistry, Springer, Cham, 545–590, https://doi.org/10.1007/978-3-319-61667-4_8, 2018.

Bartoli, O., Cesare, B., Poli, S., Acosta-Vigil, A., Esposito, R., Turina, A., Bodnar, R. J., Angel, R. J., and Hunter, J.: Nanogranite inclusions in migmatitic garnet: Behaviour during piston-cylinder remelting experiments, Geofluids, 13, 405–420, https://doi.org/10.1111/gfl.12038, 2013.

Bartoli, O., Cesare, B., Remusat, L., Acosta-Vigil, A., and Poli, S.: The H_2O content of granite embryos, Earth Planet. Sc. Lett., 395, 281–290, 2014.

Bartoli, O., Acosta-Vigil, A., Ferrero, S., and Cesare, B.: Granitoid magmas preserved as melt inclusions in high-grade metamorphic rocks, Am. Mineral., 101, 1543–1559, https://doi.org/10.2138/am-2016-5541CCBYNCND, 2016.

Bartoli, O., Acosta-Vigil, A., Cesare, B., Remusat, L., Gonzalez-Cano, A., Wälle, M., Tajčmanová, L., and Langone, A.: Geochemistry of Eocene-Early Oligocene low-temperature crustal melts from Greater Himalayan Sequence (Nepal): a nanogranitoid perspective, Contrib. Mineral. Petr., 174, 82, https://doi.org/10.1007/s00410-019-1622-2, 2019.

Beard, J. S. and Lofgren, G. E.: Dehydration melting and water-saturated melting of basaltic and andesitic greenstones and amphibolites at 1, 3, and 6.9 kb, J. Petrol., 32, 365–401, https://doi.org/10.1093/petrology/32.2.365, 1991.

Bebout, G. E.: Metasomatism in Subduction Zones of Subducted Oceanic Slabs, Mantle Wedges, and the Slab-Mantle Interface, in: Metasomatism and the Chemical Transformation of Rock: The Role of Fluids in Terrestrial and Extraterrestrial Processes, Springer Berlin Heidelberg, Berlin, Heidelberg, 289–349, https://doi.org/10.1007/978-3-642-28394-9_9, 2013.

Bodinier, J. L., Vasseur, G., Vernieres, J., Dupuy, C., and Fabries, J.: Mechanisms of mantle metasomatism: Geochemical evidence from the Lherz orogenic peridotite, J. Petrol., 31, 597–628, 1990.

Bodinier, J. L., Garrido, C. J., Chanefo, I., Bruguier, O., and Gervilla, F.: Origin of pyroxenite-peridotite veined mantle by refertilization reactions: Evidence from the Ronda peridotite (Southern Spain), J. Petrol., 49, 999–1025, https://doi.org/10.1093/petrology/egn014, 2008.

Borghini, A., Ferrero, S., Wunder, B., Laurent, O., O'Brien, P. J., and Ziemann, M. A.: Granitoid melt inclusions in orogenic peridotite and the origin of garnet clinopyroxenite, Geology, 46, 1007–1010, https://doi.org/10.1130/G45316.1, 2018.

Borghini, A., Ferrero, S., Brien, P. J. O., Günter, C., Ziemann, M. A., O'Brien, P. J., Laurent, O., Günter, C., and Ziemann, M. A.: Cryptic metasomatic agent measured in situ in Variscan mantle rocks: Melt inclusions in garnet of eclogite, Granulitgebirge, Germany, J. Metamorph. Geol., 38, 207–234, https://doi.org/10.1111/jmg.12519, 2020.

Borghini, A., Nicoli, G., Ferrero, S., O'Brien, P. J., Laurent, O., Remusat, L., Borghini, G., and Milani, S.: The role of continental subduction in mantle metasomatism and carbon recycling revealed by melt inclusions in UHP eclogites, Sci. Adv., 9, eabp9482, https://doi.org/10.1126/sciadv.abp9482, 2023.

Borghini, G., Rampone, E., Zanetti, A., Class, C., Cipriani, A., Hofmann, A. W., and Goldstein, S. L.: Pyroxenite layers in the northern apennines' upper mantle (Italy)-Generation by pyroxenite melting and melt infiltration, J. Petrol., 57, 625–653, https://doi.org/10.1093/petrology/egv074, 2016.

Bose, K. and Ganguly, J.: Quartz-coesite transition revisited: Reversed experimental determination at 500–1200 °C and retrieved thermochemical properties, Am. Mineral., 80, 231–238, 1995.

Brown, M.: Some thoughts about eclogites and related rocks, Eur. J. Mineral., 35, 523–547, https://doi.org/10.5194/ejm-35-523-2023, 2023.

Carvalho, B. B., Bartoli, O., Ferri, F., Cesare, B., Ferrero, S., Remusat, L., Capizzi, L. S., and Poli, S.: Anatexis and fluid regime of the deep continental crust: New clues from melt and fluid inclusions in metapelitic migmatites from Ivrea Zone (NW Italy), J. Metamorph. Geol., 37, 1–25, https://doi.org/10.1111/jmg.12463, 2018.

Carvalho, B. B., Bartoli, O., Cesare, B., Tacchetto, T., Gianola, O., Ferri, F., Aradi, L. E., and Szabó, C.: Primary CO_2-bearing fluid inclusions in granulitic garnet usually do not survive, Earth Planet. Sc. Lett., 536, 116170, https://doi.org/10.1016/j.epsl.2020.116170, 2020.

Cesare, B., Acosta-Vigil, A., Bartoli, O., and Ferrero, S.: What can we learn from melt inclusions in migmatites and granulites?, Lithos, 239, 186–216, https://doi.org/10.1016/j.lithos.2015.09.028, 2015.

Chen, Y. X., Zheng, Y. F., Gao, X. Y., and Hu, Z.: Multiphase solid inclusions in zoisite-bearing eclogite: Evidence for partial melting of ultrahigh-pressure metamorphic rocks during continental collision, Lithos, 200–201, 1–21, https://doi.org/10.1016/j.lithos.2014.04.004, 2014.

Čopjaková, R. and Kotková, J.: Composition of barian mica in multiphase solid inclusions from orogenic garnet peridotites as evidence of mantle metasomatism in a subduction zone setting, Contrib. Mineral. Petrol., 173, 641–646, https://doi.org/10.1007/s00410-018-1534-6, 2018.

Dallai, L., Bianchini, G., Avanzinelli, R., Deloule, E., Natali, C., Gaeta, M., Cavallo, A., and Conticelli, S.: Quartz-bearing rhyolitic melts in the Earth's mantle, Nat. Commun., 13, 7765, https://doi.org/10.1038/s41467-022-35382-3, 2022.

Faryad, S. W., Jedlicka, R., and Ettinger, K.: Subduction of lithospheric upper mantle recorded by solid phase in-

clusions and compositional zoning in garnet: Example from the Bohemian Massif, Gondwana Res., 23, 944–955, https://doi.org/10.1016/j.gr.2012.05.014, 2013.

Ferrero, S. and Angel, R. J.: Micropetrology: Are inclusions grains of truth?, J. Petrol., 59, 1671–1700, https://doi.org/10.1093/petrology/egy075, 2018.

Ferrero, S., Wunder, B., Walczak, K., O'Brien, P. J., and Ziemann, M. A.: Preserved near ultrahigh-pressure melt from continental crust subducted to mantle depths, Geology, 43, 447–450, https://doi.org/10.1130/G36534.1, 2015.

Ferrero, S., Ziemann, M. A., Angel, R. J., O'Brien, P. J., and Wunder, B.: Kumdykolite, kokchetavite, and cristobalite crystallized in nanogranites from felsic granulites, Orlica-Snieznik Dome (Bohemian Massif): not an evidence for ultrahigh-pressure conditions, Contrib. Mineral. Petrol., 171, 1–12, https://doi.org/10.1007/s00410-015-1220-x, 2016.

Ferrero, S., O'Brien, P. J., Borghini, A., Wunder, B., Wälle, M., Günter, C., and Ziemann, M. A.: A treasure chest full of nanogranitoids: an archive to investigate crustal melting in the Bohemian Massif, in: Metamorphic Geology: Microscale to Mountain Belts, Geol. Soc. Lond. Spec. Publ., 478, 13–38, https://doi.org/10.1144/SP478.19, 2018.

Ferrero, S., Wannhoff, I., Laurent, O., Yakymchuk, C., Darling, R., Wunder, B., Borghini, A., and O'Brien, P. J.: Embryos of TTGs in Gore Mountain garnet megacrysts from water-fluxed melting of the lower crust, Earth Planet. Sc. Lett., 569, 117058, https://doi.org/10.1016/j.epsl.2021.117058, 2021a.

Ferrero, S., Ague, J. J., O'Brien, P. J., Wunder, B., Remusat, L., Ziemann, M. A., and Axler, J.: High pressure, halogen-bearing melt preserved in ultra-high temperature felsic granulites of the Central Maine terrane, Connecticut (US), Am. Mineral., 106, 1225–1236, https://doi.org/10.2138/am-2021-7690, 2021b.

Ferrero, S., Borghini, A., Remusat, L., Nicoli, G., Wunder, B., and Braga, R.: H_2O and Cl in deep crustal melts: the message of melt inclusions in metamorphic rocks, Europ. J. Mineral., 35, 1031–1049, https://doi.org/10.5194/ejm-35-1031-2023, 2023.

Ferri, F., Cesare, B., Bartoli, O., Ferrero, S., Palmeri, R., Remusat, L., and Poli, S.: Melt inclusions at Mt. Edixon (Antartica): Chemistry, petrology and implications for the evolution of the Lantmann range, Lithos, 374/375, 105685, https://doi.org/10.1016/j.lithos.2020.105685, 2020.

Franke, W.: The mid-European segment of the Variscides: tectonostratigraphic units, terrane boundaries and plate tectonic evolution, Geol. Soc. Lond. Spec. Publ., 179, 35–61, https://doi.org/10.1144/gsl.sp.2000.179.01.05, 2000.

Frezzotti, M. L., Tecce, F., and Casagli, A.: Raman spectroscopy for fluid inclusion analysis, J. Geochem. Explor., 112, 1–20, https://doi.org/10.1016/j.gexplo.2011.09.009, 2012.

Frost, B. R. and Frost, C. D.: A geochemical classification for feldspathic igneous rocks, J. Petrol., 49, 1955–1969, https://doi.org/10.1093/petrology/egn054, 2008.

Gao, X. Y., Zheng, Y. F., and Chen, Y. X.: Dehydration melting of ultrahigh-pressure eclogite in the Dabie orogen: Evidence from multiphase solid inclusions in garnet, J. Metamorph. Geol., 30, 193–212, https://doi.org/10.1111/j.1525-1314.2011.00962.x, 2012.

Gao, X. Y., Zheng, Y. F., Chen, Y. X., and Hu, Z.: Trace element composition of continentally subducted slab-derived melt: Insight from multiphase solid inclusions in ultrahigh-pressure eclogite in the Dabie orogen, J. Metamorph. Geol., 31, 453–468, https://doi.org/10.1111/jmg.12029, 2013.

Gao, X. Y., Zheng, Y. F., Chen, Y. X., and Hu, Z.: Composite carbonate and silicate multiphase solid inclusions in metamorphic garnet from ultrahigh-P eclogite in the Dabie orogen, J. Metamorph. Geol., 32, 961–980, https://doi.org/10.1111/jmg.12102, 2014.

Gianola, O., Bartoli, O., Ferri, F., Galli, A., Ferrero, S., Capizzi, L. S., Liebske, C., and Remusat: Anatectic melt inclusions in ultra high temperature granulites, J. Metamorph. Geol., 39, 321–342 https://doi.org/10.1111/jmg.12567, 2020.

Golovin, A. V and Sharygin, V. V: Petrogenetic analysis of fluid and melt inclusions in minerals from mantle xenoliths from the Bele pipe basanites (North Minusa depression), Russ. Geol. Geophys., 48, 811–824, 2007.

Guillong, M., Meier, D. L., Allan, M. M., Heinrich, C. A., and Yardley, B. W. D.: SILLS: A Matlab-based program for the reduction of laser ablation ICP–MS data of homogeneous materials and inclusions, Mineral. Assoc. Can.Short Cours., 40, 328–333, 2008.

Guzmics, T., Zajacz, Z., Kodolányi, J., Halter, W., and Szabó, C.: LA-ICP-MS study of apatite- and K feldspar-hosted primary carbonatite melt inclusions in clinopyroxenite xenoliths from lamprophyres, Hungary: Implications for significance of carbonatite melts in the Earth's mantle, Geochim. Cosmochim. Ac., 72, 1864–1886, https://doi.org/10.1016/j.gca.2008.01.024, 2008.

Hagen, B., Hoernes, S., and Rötzler, J.: Geothermometry of the ultrahigh-temperature Saxon granulites revisited, Part II: Thermal peak conditions and cooling rates inferred from oxygen-isotope fractionations, Europ. J. Mineral., 20, 1117–1133, https://doi.org/10.1127/0935-1221/2008/0020-1858, 2008.

Halter, W. E., Pettke, T., Heinrich, C. A., and Rothen-Rutishauser, B.: Major to trace element analysis of melt inclusions by laser-ablation ICP-MS: methods of quantification, Chem. Geol., 183, 63–86, https://doi.org/10.1016/S0009-2541(01)00372-2, 2002.

Hanley, J. J. and Koga, K. T.: Halogens in terrestrial and cosmic geochemical systems: Abundances, geochemical behaviours, and analytical methods, Springer Geochemistry, Springer, Cham, 21–121, https://doi.org/10.1007/978-3-319-61667-4_2, 2018.

Harlov, D. E. and Aranovich, L.: The role of halogens in terrestrial and extraterrestrial geochemical processes: surface, crust, and mantle, Springer, https://doi.org/10.1007/978-3-319-61667-4, 2018.

Harlov, D. E. and Austrheim, H.: Metasomatism and the chemical transformation of rock: Rock-mineral-fluid interaction in terrestrial and extraterrestrial environments, in: Metasomatism and the Chemical Transformation of Rock: The Role of Fluids in Terrestrial and Extraterrestrial Processes, Springer Berlin Heidelberg, Berlin, Heidelberg, 1–16, https://doi.org/10.1007/978-3-642-28394-9_1, 2013.

Hermann, J.: Allanite: thorium and light rare earth element carrier in subducted crust, Chem Geol, 192, 289–306, 2002.

Hughes, L., Burgess, R., Chavrit, D., Pawley, A., Tartèse, R., Droop, G., Ballentine, C. J., and Lyon, I.: Halogen behaviour in subduction zones: Eclogite facies rocks from the Western and Central Alps, Geochim. Cosmochim. Ac., 243, 1–23, https://doi.org/10.1016/j.gca.2018.09.024, 2018.

Hughes, L., Cuthbert, S., Quas-Cohen, A., Ruzié-Hamilton, L., Pawley, A., Droop, G., Lyon, I., Tartèse, R., and Burgess, R.: Halogens in eclogite facies minerals from

the Western Gneiss Region, Norway, Minerals, 11, 1–33, https://doi.org/10.3390/min11070760, 2021.

Jochum, K. P., Weis, U., Stoll, B., Kuzmin, D., Yang, Q., Raczek, I., Jacob, D. E., Stracke, A., Birbaum, K., Frick, D. A., Günther, D., and Enzweiler, J.: Determination of reference values for NIST SRM 610–617 glasses following ISO guidelines, Geostand. Geoanal. Res., 35, 397–429, https://doi.org/10.1111/j.1751-908X.2011.00120.x, 2011.

Johannes, W. and Holtz, F.: Petrogenesis and Experimental Petrology of Granitic Rocks, Springer, Berlin, https://doi.org/10.1007/978-3-642-61049-3, 1996.

John, T., Gussone, N., Podladchikov, Y. Y., Bebout, G. E., Dohmen, R., Halama, R., Klemd, R., Magna, T., and Seitz, H. M.: Volcanic arcs fed by rapid pulsed fluid flow through subducting slabs, Nat. Geosci., 5, 489–492, https://doi.org/10.1038/ngeo1482, 2012.

Kendrick, M. A., Woodhead, J. D., and Kamenetsky, V. S.: Tracking halogens through the subduction cycle, Geology, 40, 1075–1078, https://doi.org/10.1130/G33265.1, 2012.

Klemd, R.: Metasomatism During High-Pressure Metamorphism: Eclogites and Blueschist-Facies Rocks, in: Metasomatism and the Chemical Transformation of Rock: The Role of Fluids in Terrestrial and Extraterrestrial Processes, Springer Berlin Heidelberg, Berlin, Heidelberg, 351–413, https://doi.org/10.1007/978-3-642-28394-9_10, 2013.

Kobayashi, M., Sumino, H., Burgess, R., Nakai, S., Iizuka, T., Nagao, J., Kagi, H., Nakamura, M., Takahashi, E., Kogiso, T., and Ballentine, C. J.: Halogen heterogeneity in the lithosphere and evolution of mantle halogen abundances inferred from intraplate mantle xenoliths, Geochem. Geophy. Geosy., 20, 952–973, https://doi.org/10.1029/2018GC007903, 2019.

Kotková, J., O'Brien, P. J., and Ziemann, M. A.: Diamond and coesite discovered in Saxony-type granulite: Solution to the Variscan garnet peridotite enigma, Geology, 39, 667–670, https://doi.org/10.1130/G31971.1, 2011.

Lamadrid, H. M. and Steele-MacInnis, M.: Crustal melting: Deep, hot, and salty, Am. Mineral., 106, 1193–1194, https://doi.org/10.2138/am-2022-8108, 2021.

Laurie, A. and Stevens, G.: Water-present eclogite melting to produce Earth's early felsic crust, Chem. Geol., 314–317, 83–95, https://doi.org/10.1016/j.chemgeo.2012.05.001, 2012.

Li, H. and Hermann: Chlorine and fluorine partitioning between apatite and sediment melt at 2.5 GPa, 800 °C: A new experimentally derived thermodynamic model, Am. Mineral., 102, 580–594, https://doi.org/10.2138/am-2017-5891, 2017.

Liptai, N., Berkesi, M., Patkó, L., Bodnar, R. J., O'Reilly, S. Y., Griffin, W. L., and Szabó, C.: Characterization of the metasomatizing agent in the upper mantle beneath the northern Pannonian Basin based on Raman imaging, FIB-SEM, and LA-ICP-MS analyses of silicate melt inclusions in spinel peridotite, Am. Mineral., 106, 685–700, https://doi.org/10.2138/am-2021-7292, 2021.

Liu, P., Zhang, J., Massonne, H. J., and Jin, Z.: Polyphase solid-inclusions formed by interactions between infiltrating fluids and precursor minerals enclosed in garnet of UHP rocks from the Dabie Shan, China, Am. Mineral., 103, 1663–1673, https://doi.org/10.2138/am-2018-6395, 2018.

Malaspina, N., Hermann, J., Scambelluri, M., and Compagnoni, R.: Polyphase inclusions in garnet-orthopyroxenite (Dabie Shan, China) as monitors for metasomatism and fluid-related trace element transfer in subduction zone peridotite, Earth Planet. Sc. Lett., 249, 173–187, https://doi.org/10.1016/j.epsl.2006.07.017, 2006.

Malaspina, N., Hermann, J., and Scambelluri, M.: Fluid/mineral interaction in UHP garnet peridotite, Lithos, 107, 38–52, https://doi.org/10.1016/j.lithos.2008.07.006, 2009.

Massonne, H. J. and Bautsch, H. J.: An unusual garnet pyroxenite from the Granulitgebirge, Germany: Origin in the transition zone (> 400 km depths) or in a shallower upper mantle region?, Int. Geol. Rev., 44, 779–796, https://doi.org/10.2747/0020-6814.44.9.779, 2002.

Massonne, H.-J. J.: First find of coesite in the ultrahigh-pressure metamorphic area of the central Erzgebirge, Germany, Europ. J. Mineral., 13, 565–570, https://doi.org/10.1127/0935-1221/2001/0013-0565, 2001.

Matusiak-Małek, M., Puziewicz, J., Ntaflos, T., Grégoire, M., and Downes, H.: Metasomatic effects in the lithospheric mantle beneath the NE Bohemian Massif: A case study of Lutynia (SW Poland) peridotite xenoliths, Lithos, 117, 49–60, https://doi.org/10.1016/j.lithos.2010.02.005, 2010.

McDonough, W. F. and Sun, S.-S.: The composition of the Earth, Chem. Geol., 120, 223–253, 1995.

Morgan, G. B. and London, D.: Effect of current density on the electron microprobe analysis of alkali aluminosilicate glasses, Am. Mineral., 90, 1131–1138, 2005.

Naemura, K., Ikuta, D., Kagi, H., Odake, S., Ueda, T., Ohi, S., Kobayashi, T., Svojtka, M., and Hirajima, T.: Diamond and other possible ultradeep evidence discovered in the orogenic spinel-garnet peridotite from the Moldanubian Zone of the Bohemian Massif, Czech Republic, in: Ultrahigh-Pressure Metamorphism, Elsevier, 77–111, https://doi.org/10.1016/B978-0-12-385144-4.00002-3, 2011.

Naemura, K., Hirajima, T., Svojtka, M., Shimizu, I., and Iizuka, T.: Fossilized melts in mantle wedge peridotites, Sci. Rep., 8, 1–12, https://doi.org/10.1038/s41598-018-28264-6, 2018.

Nasdala, L. and Massonne, H.-J.: Microdiamonds from the Saxonian Erzgebirge, Germany: In situ micro-Raman characterisation, Europ. J. Mineral., 12, 495–498, https://doi.org/10.1127/0935-1221/2000/0012-0495, 2000.

Németh, B., Török, K., Bali, E., Zajacz, Z., Fodor, L., and Szabó, C.: Melt-rock interaction in the lower crust based on silicate melt inclusions in mafic garnet granulite xenoliths, Bakony–Balaton Highland Volcanic Field (Hungary), Geol. Carpath., 72, 232–252, https://doi.org/10.31577/GEOLCARP.72.3.4, 2021.

Nicoli, G. and Ferrero, S.: Nanorocks, volatiles and plate tectonics, Geosci. Front., 12, 101188, https://doi.org/10.1016/j.gsf.2021.101188, 2021.

Nicoli, G., Gresky, K., and Ferrero, S.: Mesoarchean melt and fluid inclusions in garnet from the Kangerlussuaq basement, Southeast Greenland, Mineralogia, 53, 1–9, https://doi.org/10.2478/mipo-2022-0001, 2022a.

Nicoli, G., Borghini, A., and Ferrero, S.: The carbon budget of crustal reworking during continental collision: Clues from nanorocks and fluid inclusions, Chem. Geol., 608, 121025, https://doi.org/10.1016/j.chemgeo.2022.121025, 2022b.

O'Brien, P. J.: The fundamental Variscan problem: High-temperature metamorphism at different depths and high-pressure metamorphism at different temperatures, Geol. Soc. Spec. Publ.,

179, 369–386, https://doi.org/10.1144/GSL.SP.2000.179.01.22, 2000.

O'Brien, P. J.: Type-locality granulites: High-pressure rocks formed at eclogite-facies conditions, Mineral. Petrol., 86, 161–175, https://doi.org/10.1007/s00710-005-0108-2, 2006.

O'Brien, P. J.: Challenges in high-pressure granulite metamorphism in the era of pseudosections: Reaction textures, compositional zoning and tectonic interpretation with examples from the Bohemian Massif, J. Metamorph. Geol., 26, 235–251, https://doi.org/10.1111/j.1525-1314.2007.00758.x, 2008.

O'Brien, P. J. and Carswell, D. A.: Tectonometamorphic evolution of the Bohemian Massif: Evidence from high-pressure metamorphic rocks, Geol. Rundsch., 82, 531–555, 1993.

O'Brien, P. J. and Rötzler, J.: High-pressure granulites: Formation, recovery of peak conditions and implications for tectonics, J. Metamorph. Geol., 21, 3–20, https://doi.org/10.1046/j.1525-1314.2003.00420.x, 2003.

O'Reilly, S. Y. and Griffin, W. L.: Mantle metasomatism, Metasomatism and the chemical transformation of rock, Lecture Notes in Earth System Sciences, Springer, Berlin, Heidelberg, 471–533, https://doi.org/10.1007/978-3-642-28394-9_12, 2013.

Pagé, L., Hattori, K., Hoog, J. C. M. De, and Okay, A. I.: Halogen (F, Cl, Br, I) behaviour in subducting slabs: A study of lawsonite blueschists in western Turkey, Earth Planet. Sc. Lett., 442, 133–142, 2016.

Perraki, M. and Faryad, S. W.: First finding of microdiamond, coesite and other UHP phases in felsic granulites in the Moldanubian Zone: Implications for deep subduction and a revised geodynamic model for Variscan Orogeny in the Bohemian Massif, Lithos, 202/203, 157–166, https://doi.org/10.1016/j.lithos.2014.05.025, 2014.

Plank, T. and Langmuir, C. H.: The chemical composition of subducting sediment and its consequences for the crust and mantle, Chem. Geol., 145, 325–394, 1998.

Puziewicz, J., Matusiak-Małek, M., Ntaflos, T., Grégoire, M., Kaczmarek, M. A., Aulbach, S., Ziobro, M., and Kukuła, A.: Three major types of subcontinental lithospheric mantle beneath the Variscan orogen in Europe, Lithos, 362–363, 105467, https://doi.org/10.1016/j.lithos.2020.105467, 2020.

Rapp, R. P. and Watson, E. B.: Dehydration melting of metabasalt at 8–32 kbar: Implications for continental growth and crust-mantle recycling, J. Petrol., 36, 891–931, https://doi.org/10.1093/petrology/36.4.891, 1995.

Rapp, R. P., Watson, E. B., and Miller, C. F.: Partial melting of amphibolite/eclogite and the origin of Archean trondhjemites and tonalites, Precambrian. Res., 51, 1–25, https://doi.org/10.1016/0301-9268(91)90092-O, 1991.

Reinhardt, J. and Kleemann, U.: Extensional unroofing of granulitic lower crust and related low-pressure, high-temperature metamorphism in the Saxonian Granulite Massif, Germany, Tectonophysics, 238, 71–94, https://doi.org/10.1016/0040-1951(94)90050-7, 1994.

Rötzler, J. and Romer: *P-T-t* Evolution of ultrahigh-temperature granulites from the Saxon Granulite Massif, Germany, Part I: Petrology, J. Petrol., 42, 1995–2013, 2001.

Rötzler, J., Hagen, B., and Hoernes, S.: Geothermometry of the ultrahigh-temperature Saxon granulites revisited, Part I: New evidence from key mineral assemblages and reaction textures, Europ. J. Mineral., 20, 1097–1115, https://doi.org/10.1127/0935-1221/2008/0020-1857, 2008.

Rudnick, R. L. and Gao, S.: Composition of the Continental Crust, Treat. Geochem., 3, 1–64, https://doi.org/10.1016/B0-08-043751-6/03016-4, 2003.

Safonov, O. G., Tatarinova, D. S., van Reenen, D. D., Golunova, M. A., and Yapaskurt, V. O.: Fluid-assisted interaction of peraluminous metapelites with trondhjemitic magma within the Petronella shear-zone, Limpopo Complex, South Africa, Precambrian. Res., 253, 114–145, https://doi.org/10.1016/j.precamres.2014.06.006, 2014.

Sajona, F. G., Maury, R. C., Prouteau, G., Cotten, J., Schiano, P., Bellon, H., and Fontaine, L.: Slab melt as metasomatic agent in island arc magma mantle sources, Negros and Batan (Phillipines), Island Arc., 9, 472–486, https://doi.org/10.1111/j.1440-1738.2000.00295.x, 2000.

Schiano, P., Clocchiattit, R., Shimizut, N., Maury, R. C., Hofmann, K. P. J. B. A. W., Clocchiatti, R., Shimizu, N., Maury, R. C., Jochum, K. P., and Hofmann, A. W.: Hydrous, silica-rich melts in the sub-arc mantle and their relationship with erupted arc lavas, Nature, 377, 595–600, https://doi.org/10.1038/377595a0, 1995.

Schmädicke, E., Gose, J., and Will, T. M.: The P-T evolution of ultra high temperature garnet-bearing ultramafic rocks from the Saxonian Granulitgebirge Core Complex, Bohemian Massif, J. Metamorph. Geol., 28, 489–508, https://doi.org/10.1111/j.1525-1314.2010.00876.x, 2010.

Schmidt, M. W., Vielzeuf, D., and Auzanneau, E.: Melting and dissolution of subducting crust at high pressures: The key role of white mica, Earth Planet. Sc. Lett., 228, 65–84, https://doi.org/10.1016/j.epsl.2004.09.020, 2004.

Schönig, J., von Eynatten, H., Meinhold, G., Lünsdorf, N. K., Willner, A. P., and Schulz, B.: Deep subduction of felsic rocks hosting UHP lenses in the central Saxonian Erzgebirge: Implications for UHP terrane exhumation, Gondwana Res., 98, 320–323, https://doi.org/10.1016/j.gr.2020.12.029, 2021.

Schulmann, K., Lexa, O., Janoušek, V., Lardeaux, J. M., and Edel, J. B.: Anatomy of a diffuse cryptic suture zone: An example from the Bohemian Massif, European Variscides, Geology, 42, 275–278, https://doi.org/10.1130/G35290.1, 2014.

Scott, J. M., Konrad-Schmolke, M., O'Brien, P. J., and Günter, C.: High-T, low-P formation of rare olivine-bearing symplectites in Variscan eclogite, J. Petrol., 54, 1375–1398, https://doi.org/10.1093/petrology/egt015, 2013.

Skjerlie, K. P. and Patiño Douce, A. E.: The Fluid-absent Partial Melting of a Zoisite-bearing Quartz Eclogite from 1.0 to 3.2 GPa; Implications for Melting in Thickened Continental Crust and for Subduction-zone Processes, J. Petrol., 43, 291–314, https://doi.org/10.1093/petrology/43.2.291, 2002.

Skora, S., Blundy, J. D., Brooker, R. A., Green, E. C. R., de Hoog, J. C. M., and Connolly, J. A. D.: Hydrous phase relations and trace element partitioning behaviour in calcareous sediments at subduction-zone conditions, J. Petrol., 56, 953–980, https://doi.org/10.1093/petrology/egv024, 2015.

Spear, F. S. and Pyle, J. M.: Apatite, monazite, and xenotime in metamorphic rocks, Rev. Mineral. Geochem., 481, 293–335, 2002.

Stepanov, A. S., Hermann, J., Rubatto, D., Korsakov, A. V, and Danyushevsky, L. V: Melting history of an ultrahigh-pressure paragneiss revealed by multiphase solid inclusions in gar-

net, Kokchetav Massif, Kazakhstan, J. Petrol., 57, 1531–1554, https://doi.org/10.1093/petrology/egw049, 2016.

Sun, S.-S. and McDonough, W. F.: Chemical and isotopic systematics of oceanic basalts: Implications for mantle composition and processes, Geol. Soc. Lond. Spec. Publ., 42, 313–345, https://doi.org/10.1144/GSL.SP.1989.042.01.19, 1989.

Svensen, H., Jamtveit, B., Banks, D. A., and Austrheim, H.: Halogen contents of eclogite facies fluid inclusions and minerals: Caledonides, western Norway, J. Metamorph. Geol., 19, 165–178, 2001.

Svojtka, M., Ackerman, L., Medaris, L. G., Hegner, E., Valley, J. W., Hirajima, T., Jelínek, E., and Hrstka, T.: Petrological, geochemical and Sr-Nd-O isotopic constraints on the origin of garnet and spinel pyroxenites from the Moldanubian zone of the Bohemian Massif, J. Petrol., 57, 897–920, https://doi.org/10.1093/petrology/egw025, 2016.

Urann, B. M., Roux, V. Le, John, T., Beaudoin, G. M., and Barnes, J. D.: The distribution and abundance of halogens in eclogites: An in situ SIMS perspective of the Raspas Complex (Ecuador), Am. Mineral., 105, 307–318, https://doi.org/10.2138/am-2020-6994, 2020.

Vrijmoed, J. C., Austrheim, H., John, T., Hin, R. C., Corfu, F., and Davies, G. R.: Metasomatism in the ultrahigh-pressure Svartberget garnet-peridotite (Western Gneiss Region, Norway): Implications for the transport of crust-derived fluids within the mantle, J. Petrol., 54, 1815–1848, https://doi.org/10.1093/petrology/egt032, 2013.

Warr, L. N.: IMA–CNMNC approved mineral symbols, Mineral. Mag., 85, 291–320, https://doi.org/10.1180/mgm.2021.43, 2021.

Wulff-Pedersen, E., Neumann, E. R., and Jensen, B. B.: The upper mantle under La Palma, Canary Islands: Formation of Si–K–Na-rich melt and its importance as a metasomatic agent, Contrib. Mineral. Petrol., 125, 113–139, https://doi.org/10.1007/s004100050210, 1996.

Zanetti, A., Mazzucchelli, M., Rivalenti, G., and Vannucci, R.: The Finero phlogopite-peridotite massif: An example of subduction-related metasomatism, Contrib. Mineral. Petrol., 134, 107–122, https://doi.org/10.1007/s004100050472, 1999.

Zelinkova, T., Racek, M., and Abart, R.: Compositional trends in Ba-, Ti-, and Cl-rich micas from metasomatized mantle rocks of the Gföhl Unit, Bohemian Massif, Austria, Am. Mineral., 108, 1840–1851, https://doi.org/10.2138/am-2022-8746, 2023.

Zhao, Y., Zheng, J. P., and Xiong, Q.: Prolonged slab-derived silicate and carbonate metasomatism of a cratonic mantle wedge (Maowu ultramafic body, China), J. Petrol., 62, 1–25, https://doi.org/10.1093/petrology/egab081, 2021.

Zheng, Y. and Hermann, J.: Geochemistry of continental subduction-zone fluids, Earth Planet. Space, 66, 1–16, https://doi.org/10.1186/1880-5981-66-93, 2014.